

QATAR UNIVERSITY

COLLEGE OF ENGINEERING

REDUCED GRAPHENE OXIDE INCORPORATED GELMA HYDROGEL PROMOTES

ANGIOGENESIS FOR WOUND HEALING APPLICATIONS

BY

RAZA UR REHMAN SYED

A Thesis Submitted to  
the Faculty of the College of Engineering  
in Partial Fulfillment of the Requirements for the Degree of  
Masters of Science in Mechanical Engineering

June 2019

© Year. 2019 RAZA UR REHMAN SYED. All Rights Reserved.

## COMMITTEE PAGE

The members of the Committee approve the Thesis of  
RAZA UR REHMAN SYED defended on [Defense Date].

---

Dr. Anwarul Hasan  
Thesis/Dissertation Supervisor

---

Dr. Aziz ur Rehman  
Committee Member

---

Dr. John John Cabibihan  
Committee Member

---

Name  
Committee Member

---

Add Member

Approved:

---

Abdel Magid Hamouda , Dean, College of Engineering

## ABSTRACT

NAME: RAZA UR REHMAN SYED., Masters : June : [2019],  
Masters of Science in Mechanical Engineering

Title: REDUCED GRAPHENE OXIDE INCORPORATED GELMA HYDROGEL  
PROMOTES ANGIOGENESIS FOR WOUND HEALING APPLICATIONS

Supervisor of Thesis: MD. Anwarul Hasan.

Non-healing or slow healing of chronic wounds is among the serious complications of diabetes. The decrease in blood supply due to lack of angiogenesis leads to reduced supply of oxygen, nutrients and growth factors resulting in decreased proliferation and migration of endothelial cells involved in formation of blood vessels. The absence of vascular network also decreases the number of fibroblasts and keratinocyte cells in wounded area and therefore results in low collagen deposition in diabetic wounds. In this study, we report the development of rGO nanoparticles impregnated GelMa hydrogels where rGO nanoparticles were used for enhancing angiogenesis and GelMa hydrogel was applied for promoting the growth of tissue forming cells for wound healing applications. Gelatin methacrylate (GelMA) based hydrogels loaded with different concentration of rGO nanoparticles were synthesized by UV crosslinking. Characterization of rGO incorporated GelMA hydrogel retained excellent porous structure and hydrophilic properties (porosity, degradation, and swelling). *In vitro* cytotoxicity studies (Live/Dead and MTT assays), using three different cell lines, confirmed that the hydrogels are biocompatible. The GelMA hydrogel containing 2% rGO enhanced the proliferation of the cells (fibroblasts, Endothelial cells, Keratinocytes) and significant wound healing was observed in wound healing scratch assay. *In vivo* using the chick chorioallantoic membrane model showed that the presence of rGO in the GelMA hydrogel significantly enhanced angiogenesis.

## DEDICATION

*This thesis is dedicated to my beloved mother Sarwari Khatoon Shammi and my father Syed Habib ur Rehman for their endless efforts and being the best parents in the world. Without whom none of my success would be possible.*

## ACKNOWLEDGMENTS

I am very grateful to my supervisor, Dr Anwarul Hasan for being so supportive from the first day of my research work and course studies. Also, I am very thankful to my co-supervisor Dr Aziz Rahman for supervising my research at Texas A&M University at Qatar and his guidance and support.

I would like to thanks my Mentor Dr. Robin Augustine and Dr. Rashid Ahmed, for supporting and guide me in making the whole course of this thesis possible.

This project was carried out in the Mechanical and Industrial Engineering Department of Qatar University. The author is grateful to the university and the department who supported the project.

Special thanks to Qatar University Biomedical Research Center (BRC), Center of Advanced Materials (CAM), Central Lab Unit (CLU), and Environmental Science Center (ESC) for allowing to do research in their laboratories.

The author would like to acknowledge the financial support of the Qatar National Research Fund (a member of Qatar Foundation) through the National Priorities Research Program NPRP9-144-3-021.

## TABLE OF CONTENTS

DEDICATION .....	iii
ACKNOWLEDGMENTS .....	iv
LIST OF TABLES .....	<b>Error! Bookmark not defined.</b>
LIST OF FIGURES .....	viii
ABBREVIATIONS .....	xi
Chapter 1: Introduction .....	1
Background: .....	1
Angiogenesis .....	4
Reduced Graphene Oxide.....	5
Wound Dressings .....	6
Hydrogels .....	8
GelMA hydrogel .....	9
Nanocomposite hydrogels for wound dressing .....	10
Chapter 2: materials and methods.....	13
2.1 Materials.....	13
2.2 Preparation of Gelatin Methacrylate Pre-polymer .....	13
2.3 Preparation of GelMA hydrogel.....	13
2.3 Preparation of Nanocomposite GelMA hydrogel.....	14
2.4 Physical characterization.....	15
2.4.1 Scanning Electron Microscopy (SEM).....	15
2.4.2 X-Ray Diffraction Analysis.....	16
2.4.3 Degradation Study .....	16
2.4.4 Fourier-transform infrared spectroscopy (FTIR).....	16
2.4.5 Dynamic Mechanical Analysis (DMA).....	17
2.4.6. Thermogravimetric Analyzer (TGA).....	17
2.4.7 Swelling .....	17
2.5 <i>In vitro</i> Cytotoxicity Assay .....	18
2.5.1 MTT Assay .....	18
2.5.2 Live/Dead Cell Assay .....	18
2.6 Cell Migration.....	19
2.7 <i>In vivo</i> Model .....	19
2.7.1 CEA Assay .....	19
Chapter 3: REsults and discussion.....	21
3.1 Results of Physical Characterizations of the Samples .....	21
3.1.1 Transmission Electron Microscopic (TEM) images of rGO.....	21

3.1.2	<i>Results of X-Ray Diffraction Analysis</i> .....	21
3.1.3	Results of Fourier-Transform Infrared spectroscopy (FTIR) .....	22
3.1.4	Scanning Electron Microscopic images of prepared hydrogels.....	23
3.1.5.	Results of Degradation of Hydrogels.....	24
3.1.6	Swelling of Prepared Hydrogels .....	25
3.1.8	Results of Dynamic Mechanical Analysis (DMA) .....	26
3.2	Results of <i>in vitro</i> Cytotoxicity assays.....	27
3.2.1	Live/Dead Assay .....	27
3.2.2	MTT Cell Viability Assay .....	31
3.2.3	Results of <i>in vitro</i> Wound Healing Assay.....	34
3.2.4	Results of Chicken Embryo Angiogenesis (CEA) Study .....	38
Chapter 4:	Conclusion.....	41
4.1	Conclusions .....	41
4.2	Further Recommendations .....	43
References	.....	44
APPENDIX A:	Poster Presentation 1 .....	49
APPENDIX B:	Poster Presentation 2 .....	50
	.....	51
APPENDIX C:	Accepted Conference Article .....	51
(IEEE Conference)	.....	52

## LIST OF TABLES

Table1. The composition of hydrogels.....	15
---	----

## LIST OF FIGURES

Figure 1. Four Stages of Wound Healing .....	2
Figure 2. The process of angiogenesis .....	4
Figure 3. Reduced Graphene Oxide Powder Structure.....	6
Figure 4. Hydrogel wound dressing healing regeneration.....	8
Figure 5. Schematic representation for the fabrication of nanocomposite GelMA hydrogel and implication on chorioallantoic membrane of chicken egg model for enhanced angiogenesis.....	14
Figure 6. SEM micrograph at 10000X magnification of the surface of (A) GelMA hydrogel, (B) Cross-sectional image of GelMA hydrogel at 5000X, & (C) Cross sectional image of GelMA hydrogel at 2500X magnification.....	20
Figure 7. TEM image of amorphous GO nanoparticles at 43000X magnification (A) and 400000X magnification(B) .....	21
Figure 8. XRD curves of pure GelMA hydrogel, rGO nanoparticles, 1 wt% rGO loaded GelMA hydrogel (GrG1), 2 wt% rGO loaded GelMA hydrogel (GrG2) respectively.....	22
Figure 9. Degradation curve of rGO/GelMA hydrogel films with time. Error bars represent the SD of measurements performed on at least 5 specimens.....	23
Figure 10. The swelling percentage of GelMA hydrogel and nanocomposite GelMA hydrogel after 0, 15, 30, 60 and 120 minutes respectively.....	24
Figure 11. Fourier-transform infrared spectroscopy (FTIR) of rGO, GelMA hydrogel, 2% GO loaded GelMA hydrogel (GrG2) and 0.5 GO loaded GelMA hydrogel (GrG0.5) .....	25
Figure 12. Thermogravimetric Analysis (TGA) of 2% GO loaded GelMA hydrogel (GrG2), 0.5% GO loaded GelMA hydrogel (GrG0.5) and only GelMA hydrogel	

respectively.....26

Figure 13. The storage and loss modulus ranges in amplitude sweep test (7A) and frequency sweep test (7B) of GelMA hydrogel and 2% rGO loaded GelMA hydrogel (GrG2).....27

Figure 14. Cell viability (Live/Dead cell assay) on fibroblast for control, pure GelMA hydrogel, 1% rGO loaded GelMA hydrogel (GrG1), 2% rGO loaded GelMA hydrogel (GrG2) and 4% rGO loaded GelMA hydrogel (GrG4) respectively .....28

Figure 15. Cell viability (Live/Dead cell assay) on Keratinocytes for control, pure GelMA hydrogel, 1% rGO loaded GelMA hydrogel (GrG1), 2% rGO loaded GelMA hydrogel (GrG2) and 4% rGO loaded GelMA hydrogel (GrG4) respectively .....29

Figure 16. Cell viability (Live/Dead cell assay) on Endothelial cells for control, pure GelMA hydrogel, 1% rGO loaded GelMA hydrogel (GrG1), 2% rGO loaded GelMA hydrogel (GrG2) and 4% rGO loaded GelMA hydrogel (GrG4) respectively.....30

Figure 17. Histogram for the comparison of the MTT assay of fibroblast for 1 day, 3 days and 5 days.....31

Figure 18. Histogram for the comparison of the MTT assay of endothelial cells for 1 day, 3 days and 5 days .....32

Figure 19. Histogram for the comparison of the MTT assay of keratinocytes for 1 day, 3 days and 5 days .....33

Figure 20. Wound healing scratch assay of using fibroblast for control, GelMA hydrogel, 1% rGO loaded GelMA hydrogel (GrG1), 2% rGO loaded GelMA hydrogel (GrG2), & 4% rGO loaded GelMA hydrogel (GrG4). Percentage of wound healing was

measured and presented on histogram using ImageJ softwar .....34

Figure 21. Wound healing scratch assay of using Endothelial cells for control, GelMA hydrogel, 1% rGO loaded GelMA hydrogel (GrG1), 2% rGO loaded GelMA hydrogel (GrG2), & 4% rGO loaded GelMA hydrogel (GrG4). (D) Percentage of wound healing was measured and presented on histogram using ImageJ software (Figure 17B).  
.....35

Figure 22. Wound healing scratch assay of using Keratinocytes for control, GelMA hydrogel, 1% rGO loaded GelMA hydrogel (GrG1), 2% rGO loaded GelMA hydrogel (GrG2), & 4% rGO loaded GelMA hydrogel (GrG4). (D) Percentage of wound healing was measured and presented on histogram using ImageJ software (Figure 18B).  
.....37

Figure 23. (A) In vivo CEA assay of control, in the presence of the GelMA hydrogel. 1 wt% rGO loaded GelMA hydrogel (GrG1), and 2 wt% rGO loaded GelMA hydrogel (GrG2). Increase of matured blood vessel formation (marked by black arrows) was observed in embryo treated with GelMA hydrogel with 2 wt% rGO nanoparticles (GrG2) .....38

## ABBREVIATIONS

GelMA	Gelatin-Methacryloyl
rGO	Reduced Graphene Oxide
SEM	Scanning electron microscope
EDX	Energy-dispersive X-ray spectroscopy
FTIR	Fourier-transform infrared spectroscopy
XRD	X-ray diffraction
DSC	Differential Scanning Calorimetry
TGA	Thermogravimetric analysis
UV	Ultraviolet
DPBS	Dulbecco's Phosphate buffered saline
DMEM	Dulbecco's Modified Eagle Medium
PBS	Phosphate buffered saline
min	Minutes
hrs	Hours
FBS	Fetal bovine serum
TGF	Transforming growth factor
VEGF	Vascular Endothelial Growth Factor
<i>T</i>	Temperature
HaCat	Cultured Human Keratinocyte (cells)
3T3	3-day transfer, inoculum $3 \times 10^5$ cells.

## THESIS LAYOUT

This thesis is divided into four chapters. The sequence of the chapters are as below

Chapter 1 presents the problems and detailed introduction of the steps of wound healing. Furthermore, the literature review of wound dressing materials and use of hydrogel and reduced graphene oxide (rGO) for the development of wound dressing.

Chapter 2 explains the materials and methods for fabricate rGO incorporated nanocomposite GelMA hydrogel. After then, it describes the physical characterization approaches, then the biological characterizations using the cell culture investigation in an *In vitro* and angiogenesis activity in an *In-vivo* models.

Chapter 3 presents a thorough description of the results obtained in this study.

Chapter 4 concludes the present study with the promising potential of rGO incorporated GelMA hydrogel as a wound healing hydrogel material. In addition, it further defines the future work recommendations.

## CHAPTER 1: INTRODUCTION

### **Background:**

Delay in healing or non-healing of wounds is one of the the most widespread problem in the world associated with many pathophysiological conditions. The process of delayed healing of wounds often faces many hindrances especially in case of burn and diabetes wounds and causes serious complications. Multiple lines of evidences suggest that burden of diabetes related morbidities in wound healing is far more in terms of number of patients. A recent survey suggests that approximately, 170 million people in the world are affected by diabetes where 20.8 million people in the USA suffer from this disease and these numbers are projected to be double by 2030 [1]. Foot ulcers in diabetic patients is a leading cause of amputation. In the developed world, hospital admissions and major morbidity are mostly associated with diabetes [2], which leads to pain, suffering, and poor quality of life for the patients. 15% of the diabetic patients suffer from diabetic foot ulcers (DFUs), which leads to amputation and about 84% of all diabetic patients have lower-leg amputations [3]. The moment a diabetic patient suffers a wound in the skin of their foot, they became in danger of amputation. A delayed healing or non-healing of the wound in a person with DFUs is due to the reduction of growth factor response and decreased cells, which lead to reduced peripheral blood flow and decreased angiogenesis. The major known factors that contribute in delayed healing of wound includes, angiogenesis response [4-6], decreased growth factor production [4, 7, 8], keratinocyte, fibroblast, and endothelial cells migration and proliferation [4], quantity of granulation tissue, epidermal barrier function, collagen accumulation [4], and macrophage function [5]. The process of wound healing involves activation of endothelial, keratinocyte, and fibroblast cells,

platelets and macrophages, as a result of a cellular response to injury. And those cells release many growth factors and cytokines to contribute in the wound healing process. The natural wound healing includes cellular and molecular process [1]. The healing process depends on the interactions between cellular factors as well as the surrounding extra-cellular matrix (ECM) [3]. It includes; inflammation, cell migration, angiogenesis, synthesis of the provisional matrix, collagen deposition and re-epithelization [6]. The process of wound healing can be categorized in four steps, i.e. (i) hemostasis (ii) inflammation, (iii) proliferation and (iv) remodeling. Inflammation includes the formation of new blood vessels from the existing vasculature (angiogenesis) and proliferation includes the proliferation of fibroblast and keratinocyte cells. Delivery of healing related cells, nutrients, oxygen, cytokines to the wound area, space for new tissue formation, and cleaning of neurotic tissue in the wound area are required in the early period of wound healing [9-12]. All these processes require the formation of a blood vessel network [11]. In diabetic wounds, due to the changes in the formation of blood vessels, especially microvascular formation, the wound healing delayed and finally, an ulcer appears.

### Four Stages of Wound Healing

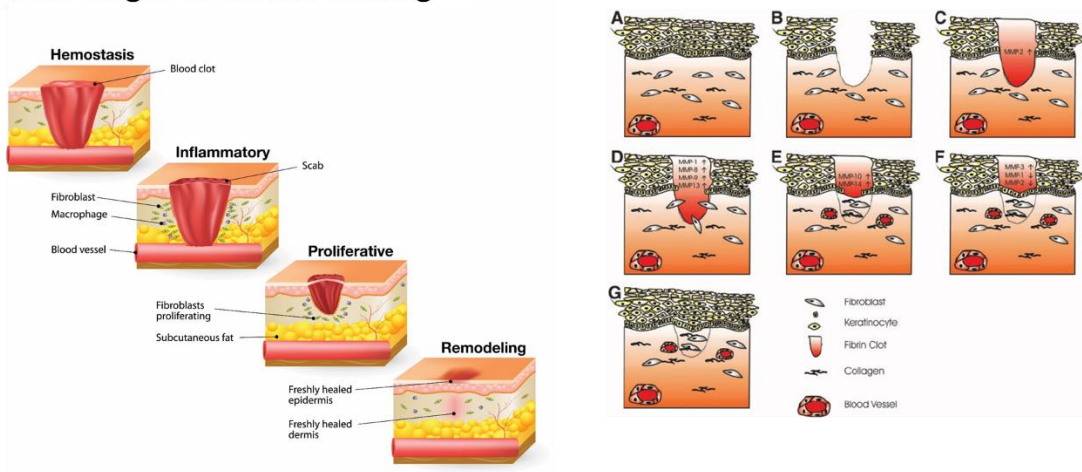


Figure 1: Four Stages of Wound Healing.

The biological tissues contain different cell types, embedded within the extracellular matrix. In order to survive and function optimally, each of those cells requires a continuous supply of nutrients and oxygen, which is being supplied by the vascular system. This also helps in removing carbon dioxide and other waste. It has been proven that the maturation of the vascular network is crucial in the wound healing process, which requires the participation of different cell types and growth factors. Current techniques to promote the maturation of vascular networks can be categorized into three types: micro engineering techniques [13, 14], cell-based techniques [15, 16] and biochemical techniques [17-19]. In micro engineering technique, vascular-like structures are synthesized within the scaffolds by using the techniques that are used in semiconductor industries for the improvement of polymers. In cell-based techniques, with the expectation of development of vascular networks *in vivo*, progenitor or mature endothelial cells are co-cultured within the scaffolds along with the cells of interest. In biochemical techniques, the small bioactive molecules or growth factors that are involved in vascularization *in vivo* are loaded in the scaffold. However, there are some limitations in all of these approaches. Such as, in micro-engineering technique there is a lack of host integration. In cell seeded technique, there is a deficiency of control over cells dissociation and differentiation. In biochemical technique, due to the short half-life of the growth factors, it degrades very fast in physiological conditions [20, 21].

In order to prevent wound expansion, the formation of the vascular network is required in the early stage of healing. Wounds generally heal faster by a moist dressing [22]. An ideal wound dressing i.e. natural skin contain 85% water content and excellent permeability [9, 23]. An effective wound dressing should have the following properties in order to promote angiogenesis and to aid healing process; (1) high-level water absorption ability, (2) maintain water balance in the wound area, (3) satisfactory

adherent for good wound-dressing contact. (4) maintain physical structure even after excessive fluid absorption, (5) biocompatible, (6) a good barrier for the infection, (7) Good antibacterial activity to prevent bacterial growth under the dressing; and (8) no cytotoxic effect.

### Angiogenesis

Angiogenesis is the process of new blood vessel formation from the existing vasculature. The term angiogenesis was first coined by Arthur Hertig in 1935 on his report of blood vessel development of in the human. The angiogenesis involves differentiation, growth, and migration of endothelial cells. Angiogenesis is triggered by various angiogenic inhibitors and stimulators. Changes in angiogenesis are proportional to the changes in the metabolic activity of the cells, and hence, proportional to the capillarity. However, in these whole procedures, oxygen plays a significant role. The recognition that angiogenesis could play a significant role in therapeutic treatment has grown a great interest during the last 40 years.

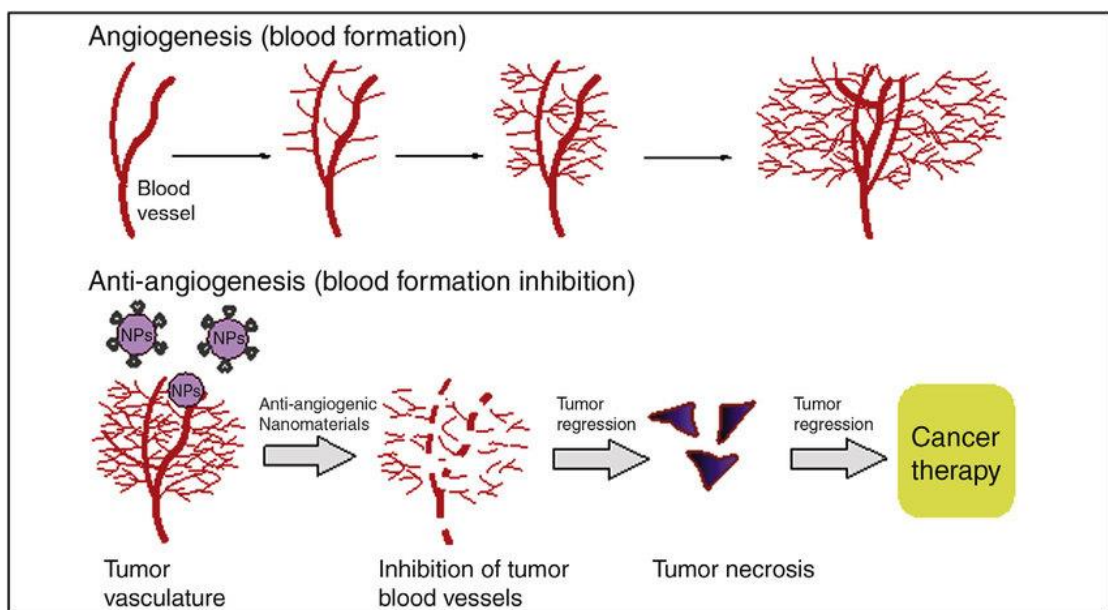


Figure 2: The process of angiogenesis.

## **Reduced Graphene Oxide**

In recent developments of nanotechnology and nanoscience various nanomaterials have been suggested for biomedical applications. Among them graphene oxide has proven to be a promising material for biomedical applications. The arrangement of Carbon atoms is in a honeycomb lattice structure in graphene, which is two-dimensional carbon nanomaterial [24-28]. Recently, Graphene and their derivatives (Graphene oxide (GO) and reduced graphene oxide (rGO)) have attracted great attention as an inorganic additive of biopolymers for the composition of novel hydrogels [29]. Their excellent fundamental properties such as biocompatibility of biopolymers, good electro thermal activity, unique chemical and electrical properties [29], and good Nano filler for enhancing polymeric materials [30] make them one of the most favorable materials for numerous biomedical applications. Graphene derivatives have significant potential in Nanomedicines [31, 32], cancer drug delivery [33], biological sensors [34], development of technology viable devices [35], cancer biomarkers [35], catalyst [31, 36], electronics [36] and better antibacterial agent [37]. Since graphite is naturally occurring material and carbon in one of the most common elements in our ecosystem, thus we can expect graphene derivatives would be more safe and useful for the biological purpose [46]. The drug delivery system based on graphene has been suggested since 2008. Graphene Oxide (GO) has high drug loading efficiency due to its very high surface area. Carbon nanotube has been used as a drug carrier including various chemotherapy drugs e.g. camptothecin (CPT) [38, 39], ellagic acid [40], SN38 (an analog of CPT) [41], doxorubicin (DOX) [40, 42] and 1,3-bis(2-chloroethyl)-1-nitrosourea (BCNU) [43], incorporated on GO with numerous functionalization on surface. GO has also been used as a biosensor for the detection of drugs [44]. It can functionalize covalently due to the presence of different chemically reactive oxygen groups e.g. epoxy, hydroxyl and carboxylic groups [45, 46]. However, GO can also be

functionalized non-covalently through p-p stacking, electrostatic binding or hydrophobic interactions [47]. Furthermore, some promising effects of cell proliferation have recently been observed by using graphene nanomaterials on various types of cells [48-51]. Sudip Mukherjee et al [52] observed angiogenic property of graphene oxide (GO) and reduced graphene oxide (rGO) through several *in vitro* and *in vivo* angiogenesis assays. They found GO and rGO exhibit pre-angiogenic property depending upon their concentrations. They also have suggested their study will be helpful in the future development of Nanomedicine. In addition, graphene oxide and its derivatives can be used in combination of other biomaterials, such as biopolymers, to make graphene oxide based nanocomposites for different biomedical applications [18, 47, 53-56]

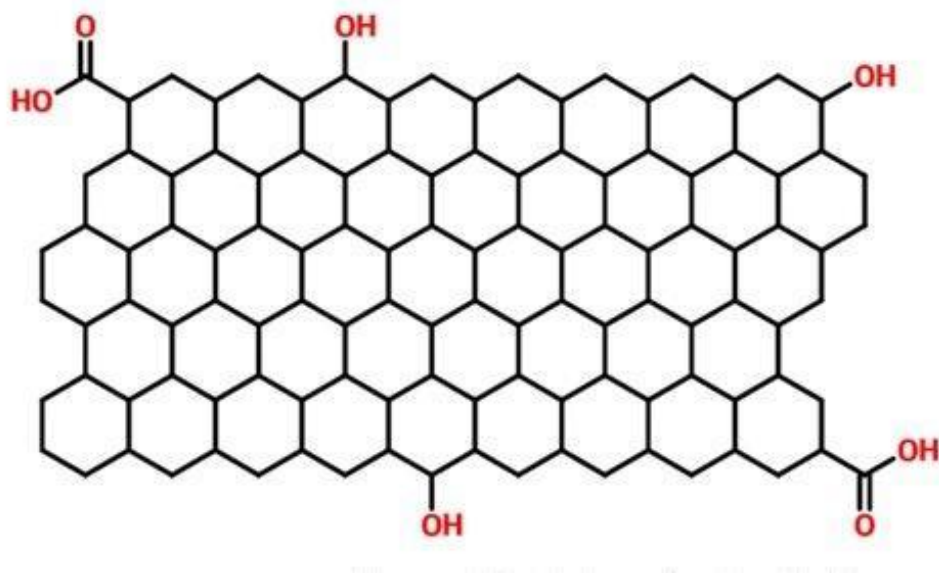


Figure 3: Reduced Graphene Oxide Powder Structure.

### Wound Dressings

The wound treatments have grown from ancient times. In the early times, the wound dressing materials were designed to protect the wound from environmental irritants and to inhibit the bleeding. For the prevention of invasion and in homeostasis skin plays an

important role by microorganisms. Once the skin gets damaged, the skin needs to be covered immediately by the dressing. Over the past few decades, the wound dressing has seen many changes. In order to cover the wound to avoid infection, several wound dressing materials have been for effective healing of wound since ancient times. Several examples of early times wound dressing materials are: animal fats, plant fibers and honey paste [57-59]. Particularly, for the diabetic foot ulcers (DFU) several wound dressing materials have been used. Nowadays, with the development in different biopolymers and fabrication techniques, the wound dressing material is expected to have some remarkable wound healing properties for the rapid healing of the wound. The choice of right biopolymers could significantly enhance the healing of wound compared to the conventional wound dressings. Some bioactive ingredients containing antibacterial, antimicrobial and anti-inflammatory properties could be added in bandages for control release in the wound. In order to aid the wound, an active wound dressing can play a significant role by controlling its biochemical processes. To design an ideal wound dressing, its physical, chemical and mechanical properties need to be considered. The ultimate objective is to get the highest healing rate of the wound.

The principle of moist wound dressing was pioneered by Winter (1962). The main function of wound dressing materials is to accelerate the wound healing process by protecting the wound, destroying the pathogenic microorganism, absorbing the extra body fluid from the wound area and by improving the appearance. The performance requirement of the wound dressing could change as the wound progress, however, it is widely accepted that a moist wound dressing could enhance the wound healing process. Taking those conditions under consideration, most of the wound dressing materials are designed. In addition to providing a physical barrier to the wound, the wound dressing material should be permeable to the oxygen and moisture. Studies have proven the

efficiency of moist wound dressing [60, 61]. Among other wound dressing materials that have been investigated, hydrogels combine the properties of a moist wound dressing with good fluid absorbance ability and transparent appearance for careful monitoring of the wound.

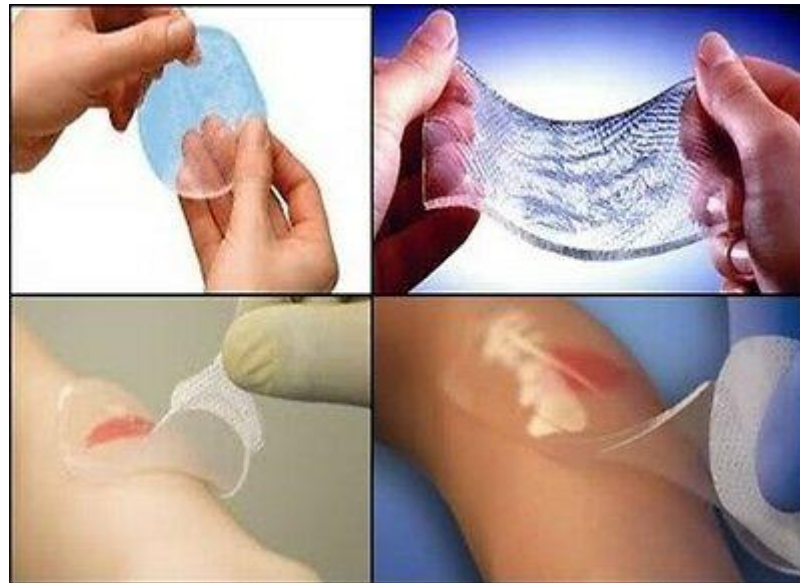


Figure 4: Hydrogel wound dressing healing regeneration.

### **Hydrogels**

Hydrogels are cross-linkable synthetic or natural polymer chain. The formation of hydrogels can be from natural or synthetic polymers. Both synthetic and natural polymers have their own limitations and benefits. The most commonly used synthetic polymers for the fabrication of hydrogels are PCL, PLGA, PVA, PEG, and PLA. Natural polymers such as chitosan, alginate, and collagen have gained popularity due to their non-immunogenic response, biodegradability and biocompatibility. However, both natural and synthetic polymers have their own limitations. Hydrogel is a material that has the ability to absorb maximum amount of water and swells eventually. The synthesis of the hydrogel is done by the formation of cross-linked polymers network

that is produced by the reaction of monomers or a polymeric material. In biomedical and tissue engineering, hydrogel has gathered significant attention by the researchers due to its wide variety of applications [62, 63]. Hydrogel has the ability to cover the irregular tissue defects and has a high degree of flexibility [64]. The properties of hydrogels mimic extracellular matrix (ECM) of the tissues and make them prominent scaffolds for biomedical applications. They have been widely applied in numerous biomedical application such as regenerative medicine, tissue engineering and controlled drug delivery [64-66]. Their excellent hydrophilic property due to the existence of hydrophilic groups, such as hydroxyl, carboxyl, amino and amido in the polymer chains, makes them more feasible for wound healing application. This water content produces a highly porous, soft and flexible structure. Hydrogels are biocompatible, non-antigenic, durable, permeable to water vapor, and maintain its physical structure even after excessive water absorption. It securely covers the wound and prevents infection by bacteria. These all together make them quite similar to natural ECM. However, an ideal hydrogel should have stronger mechanical property, excellent antimicrobial activity.

### **GelMA hydrogel**

Gelatin Methacrylate hydrogels or GelMA hydrogels have the benefits of both synthetic and natural polymers. GelMA hydrogels have highly tunable physical characteristics and suitable biological properties. They have widely used for various biomedical applications. The cell attaching and matrix metalloproteinase responsive peptide motifs which allow cells to proliferate and spread in GelMA- based scaffolds are present in GelMA hydrogel. This property makes GelMA hydrogel closely resemble to some essential properties of native Extra-Cellular Matrix (ECM). Monomers of Gelatin Methacrylate (GelMA) crosslinks when exposed to light irradiation to form GelMA hydrogel with tunable mechanical properties [67]. High Cross-linking degree of the

polymer can be obtained at a low concentration of photo-initiator within a minute or even seconds, which minimize cytotoxicity. The hydrogels pre-polymer solution of GelMA hydrogel can fill the wound according to its shape by flowing on the surface of the wound [11]. GelMA hydrogels have relative low antigenicity and significantly less expansive compared to collagen, whilst maintain the property of biocompatibility [68]. Furthermore, the transparent nature of hydrogel provides easy observation of the cellular behavior seeded onto or within the hydrogel. In addition, the degradation, biological and mechanical properties can easily be tuned by changing the GelMA concentration, methacrylation degree or photo-polymerization time. Gelatin present in GelMA hydrogels provides cell responsive features such as proper cell adhesion sites and proteolytic degradability.

#### **Nanocomposite hydrogels for wound dressing**

Nanocomposites hydrogel (NCH) are the recent development in hydrogel technology [62]. The incorporation of metal/metal oxide nanoparticles into the hydrogel network have gained great interest Research trends are significantly increased current in the incorporation of many metal/metal oxide nanoparticles into the hydrogel network [63]. Silver nanoparticles have been loaded on the surface of the material to enhance the antibacterial activities [69]. [29] In his study proved that the reactive oxygen species produced by  $Zn^{2+}$  can kill the bacteria by damaging protein and cell wall. In addition, for the surface modifications of GelMA hydrogels, a short cationic antibacterial peptide known as HHC-36 has been examined as an antimicrobial peptide [70-73]. However, these drug loading method and surface modifications are generally requiring multistep, complex procedure and are a time-consuming method. The mechanical property, at the same time, plays a significant role in directing the phenotype and genotype of the cells and regulating the interactions b/w cells and extracellular matrix (ECM). Zinc Oxide (ZnO) is the most commonly used nanoparticle for the incorporation in membranes for

wound healing applications. However, other metal oxides have been used for cartilage repair, bone regeneration, and tissue engineering applications. Using electrospinning and physical blending techniques, the PVA-alginate nanofibers mats were loaded with ZnO nanoparticles and PVA-chitosan membrane respectively. Vicentini et al. and Shalumon et al [74, 75] have observed antibacterial activity using PVA-chitosan membranes loaded with ZnO nanoparticles against *S.aureus*. Shalumon et al [74] demonstrated in his study that, chitosan-PVA-ZnO nanofibers mats exhibit antibacterial activity against both *S. aureus* and *E. coli* growth at a low concentration of ZnO nanoparticles. Whereas, at high concentration of ZnO nanoparticle the nanofibers mat didn't show antibacterial activity. However, ZnO nanoparticles enhanced thermal and mechanical properties of both membranes and nanofiber mats. ZnO loaded chitosan nanocomposite badges were prepared for wound healing and showed faster re-epithelization, collagen deposition, antibacterial activity, blood clotting rate, oxygen vapor transmission, and enhanced swelling effects [76]. Another wound dressing patch was synthesized by incorporating ZnO nanoparticle in collagen-dextran composite hydrogel membrane using glutaraldehyde crosslinker [77]. Moreover, the incorporation of ZnO nanoparticles have decreased water uptake and degradation rate of collagen. Furthermore, ZnO incorporated alginate nanocomposite hydrogel was synthesized by a freeze-drying crosslinking method for wound dressing or bandages [78]. Also, faster blood-clotting, controlled degradation rate and decreased water uptake degree were obtained by the addition of ZnO nanoparticles. At low concentration of ZnO nanoparticles alginate-ZnO nanocomposite hydrogel exhibit no cytotoxic effect, however, at a higher concentration a slight decrease in cell viability was observed. AgNO<sub>3</sub> nanoparticles were incorporated in PVA-cellulose acetate-gelatin membranes through  $\gamma$ -irradiation crosslinking and in PVA-chitosan nanofibers through

electrospinning for the synthesis of an effective wound dressing [79]. Usama et al. have incorporated GO nanoparticles in PVA/Ag/starch films for wound dressing [80]. Results depict that the addition of GO nanoparticles has significantly enhanced the antibacterial activity against *Gramm* positive and *Gramm* negative bacteria. Wen et al. have prepared a wound dressing composite membrane by carefully suspending silver sulfadiazine particles with bacterial cellulose [81].

The individual features of GelMA hydrogel and rGO nanoparticle have inspired us the feasibility of combing them to make an effective wound dressing material for wound healing application. In our present work, GelMA hydrogel with varying concentration of rGO are synthesized to get optimum concentration for enhanced angiogenesis. The individual components of the material are confirmed using different characterization methods. The cytotoxicity of GelMA hydrogel and rGO at different concentrations are observed. Finally, the angiogenic properties of the material have been demonstrated through *in vivo* angiogenesis assay. We strongly believe that our study on rGO/GelMA hydrogel will put forward the insight for the advancement of angiogenic treatment strategies for several diseases where angiogenesis plays a significant role. Moreover, this will also pave the ways in the advancement of different tissue engineering applications by making artificial tissues using GelMA hydrogel.

## CHAPTER 2: MATERIALS AND METHODS

### 2.1 Materials

Freeze-dried GelMA polymer obtained from Nano Micro Technologies and Tissue Engineering Lab of Engineering and Architecture department at AUB. Phosphate buffer saline (PBS) solution, Fatal Bovine Serum and trypsin were purchased from Gibco, USA. N-Methyl-2-pyrrolidone (NMP) from VWR, USA. Dulbecco's modified eagle medium (DMEM) was purchased from. Reduced Graphene Oxide powder from Graphite, UK. Live/Dead cell Imaging Kit from Thermo Fisher Scientific.

### 2.2 Preparation of Gelatin Methacrylate Pre-polymer

Gelatin derived from porcine skin was dissolved in PBS solution at 60 °C (25, 26). Under stirred conditions of 50 °C, 8 mL of MA was added for each 100 mL of gelatin solution at 0.5 mL/min until the target volume was reached (Figure 5). The mixture was then reacted for 3 h. 5X dilution at 40 °C was then performed by adding 400 mL of PBS preheated at 50 °C to stop the reaction. After that, salts and methacrylic acid were removed by allowing the mixture to be dialyzed against distilled water for 1 week at 40 °C. The obtained solution was freeze-dried for one week resulting in a white porous foam-like GelMA prepolymer which was kept at -80 °C until further use (23, 26, 27).

### 2.3 Preparation of GelMA hydrogel

Freeze-dried GelMA polymer (5%) with 0.5% of photoinitiator (2-hydroxy-1-[4-(2-hydroxyethoxy) phenyl]-2-methyl-1-propanone) was fully dissolved in 1 ml of PBS (1X) solution using vortex. 50 µL of the prepared solution was placed on round glass slides and then exposed to UV light (500 nm, 7 mwWcm<sup>-2</sup>). The samples were placed at 7 cm distance from the UV source and exposed for 10 seconds to crosslink the free radicals of GelMA prepolymer chains [82].

### 2.3 Preparation of Nanocomposite GelMA hydrogel

5 mg of RGO (Reduced Graphene Oxide) nanoparticles were added in 1 ml of N-Methyl-2-pyrrolidone (NMP) and dispersed very well with the vortex. The suspension was then diluted to 0.5 $\mu$ g/10 $\mu$ l, 1 $\mu$ g/10 $\mu$ l and 2 $\mu$ g/10 $\mu$ l and added in 1ml of PBS to make 1 wt%, 2 wt%, and 4 wt% nanocomposite hydrogel respectively. 5% of freeze-dried GelMA polymer and 0.5% of photo initiator was mixed with PBS containing nanoparticles separately for each set and mixed again until the GelMA polymer dissolved completely. 50 $\mu$ l of prepared solution was placed on round glass slides and exposed to UV light (500 nm, 7 mwWcm<sup>-2</sup>) for 11 seconds for crosslinking.

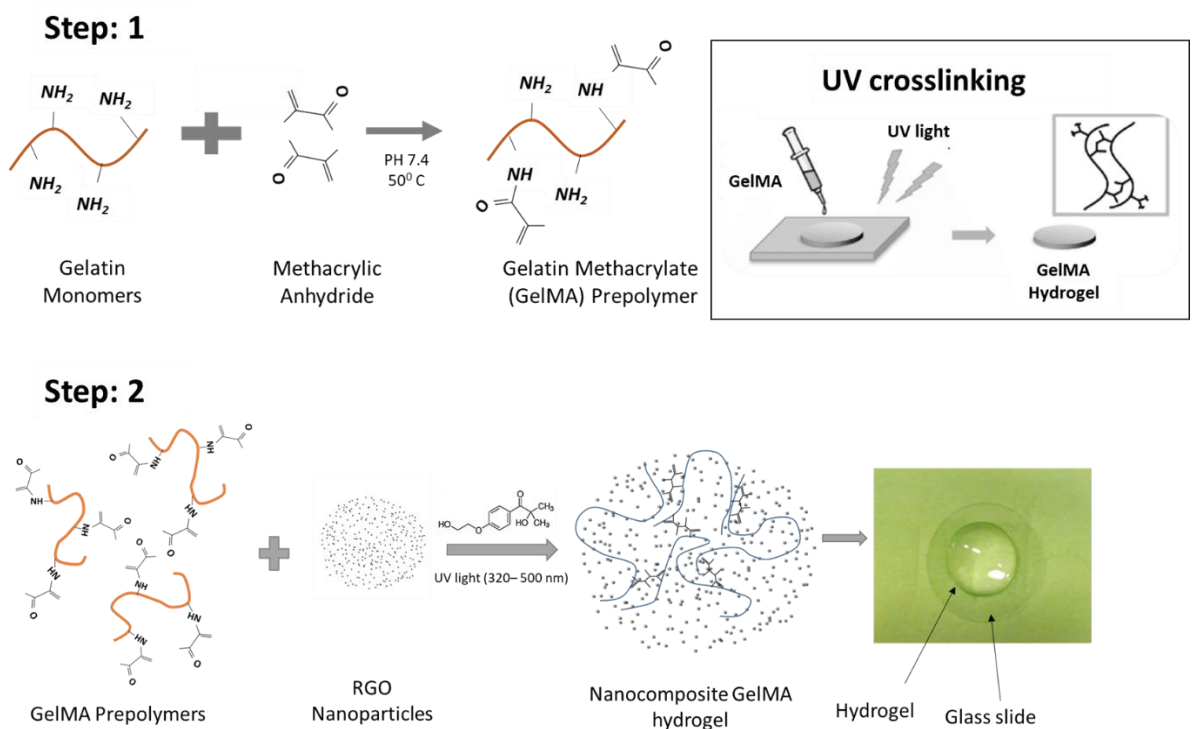


Figure 5: Schematic representation for the fabrication of nanocomposite GelMA hydrogel and implication on chorioallantoic membrane of chicken egg model for enhanced angiogenesis.

Table: 1

The composition of hydrogels.

Samples	Abbreviation	GelMA % (w/v)	rGO % (w/w)
GelMA	GelMA	5	0
GelMA 5% rGO 0.5%	GrG 0.5	5	0.5
GelMA 5% rGO 1%	GrG1	5	1
GelMA 5% rGO 2%	GrG2	5	2
GelMA 5% rGO 4%	GrG4	5	4

## 2.4 Physical characterization

### 2.4.1 Scanning Electron Microscopy (SEM)

A scanning electron microscope is a powerful tool and is being widely used for material characterization in recent years. It is an electron microscope that scan the surface of the material using electron beam to produce images of the surface. The surface morphology of GelMA hydrogel and rGO nanoparticles were observed using Scanning Electron Microscope (SEM) and Transmission Electron Microscope (TEM). GelMA hydrogels were freeze-dried until the water was evaporated or sublimed completely. Lyophilized rGO nanoparticles and GelMA hydrogel were affixed on carbon stubs. A thin layer of gold (6nm) were then coated on the samples to avoid discharging of the electron. The samples were observed using a secondary electron detector under an accelerating voltage of 20kv.

### ***2.4.2 X-Ray Diffraction Analysis***

X-Ray diffraction (XRD) is an analytical technique used for microstructure analysis. XRD pattern of the GelMA hydrogel, nanocomposite hydrogel at 1%, 2%, and 4% concentration were obtained using Regaku, Miniflex ii, XRD system. Freeze-dried hydrogel samples of 4 mg were placed into the specimen holder of XRD at room temperature (40 KV voltage, 30 mA current scanning scope of  $2\theta$  was range from  $0^\circ$  to  $60^\circ$  scanning rate of  $5^\circ/\text{min}$  to  $11^\circ$  with a step size of  $0.032^\circ$ ).

### ***2.4.3 Degradation Study***

50  $\mu\text{g}$  of GelMA hydrogel of 5% concentration and nanocomposite GelMA hydrogel of 1 wt%, 2 wt% and 4 wt% concentration of rGO nanoparticles were freeze-dried for 24 hours. Initial weight ( $W_0$ ) of all the samples were measured and then kept with PBS in an incubator at  $37^\circ\text{C}$ . The PBS was refreshed weekly. The specimens were taken out and dried under vacuum at  $59^\circ\text{C}$  at predetermined time intervals and final weight ( $W_t$ ) were observed. Data were reported as the mean  $\pm$  SD of five samples for each type. The degradation rates were measured according to the following formula:

$$\text{Degradation rate (\%)} = \frac{W_0 - W_t}{W_0} \times 100\%$$

### ***2.4.4 Fourier-transform infrared spectroscopy (FTIR)***

Using FTIR spectroscopy the chemical composition of the GelMA hydrogel, reduced graphene oxide (rGO), 0.5% rGO loaded GelMA hydrogel and 2% rGO loaded GelMA hydrogel was observed. 50  $\mu\text{l}$  of GelMA hydrogel and nanocomposite hydrogels were used for FTIR spectroscopy. Hydrogel samples were freeze-dried and the absorbance peaks of FTIR were measured on a PerkinElmer (USA), FTIR Spectrum 400. The spectra were determined over a frequency range of  $500\text{-}2000\text{ cm}^{-1}$ . It was recorded with

a resolution of  $\pm 4 \text{ cm}^{-1}$  and a scanning frequency of 32 times at room temperature.

#### ***2.4.5 Dynamic Mechanical Analysis (DMA)***

The viscoelastic behavior of the hydrogel was analyzed using dynamic mechanical analysis. GelMA hydrogel and 2% rGO loaded GelMA hydrogel was analyzed to observe the difference of viscoelastic behavior after the incorporation of reduced graphene oxide nanoparticles. Hydrogels of 2 mm thickness and 2 cm diameter were placed simultaneously between the plates of the dynamic mechanical analyzer (RSA-G2 Solids Analyzer). Amplitude sweep test and frequency sweep test were performed simultaneously. Plots of storage and loss modulus were obtained from 0.01 to 1 strain (%) for amplitude sweep test and from 0.1 to 100 Hz for the frequency sweep test.

#### ***2.4.6. Thermogravimetric Analyzer (TGA)***

In order to examine the weight loss with respect to time as temperature changes, the thermal degradation behavior of GelMA hydrogel, 05% rGO loaded GelMA hydrogel & 2% rGO loaded GelMA hydrogel was investigated by a thermogravimetric analyzer (TGA) (PerkinElmer, Pyris 6, USA). Freeze-dried samples of 50  $\mu\text{l}$  volume were heated from room temperature to 700°C with a purge of  $\text{N}_2$  at a heating rate and a flow rate of 5°C/min and 70 ml/min, respectively.

#### ***2.4.7 Swelling***

The swelling properties of GelMA hydrogel were investigated by using the gravimetric technique. Firstly, the dried samples were weighed and then placed in a petri dish filled with distilled water (DW). The Petri dishes were then placed in a temperature-controlled water bath at the room temperature. Later, the weight of swollen hydrogel samples was measured by a digital balance of Mettler Toledo after specific time intervals. After removing the sample from the water, the weight of the swollen hydrogel

was measured and then dried with a filter paper to remove excess water. The swelling property was then calculated by using the following formula

$$Q(g/g) = (W_{wet} - W_{dry})/W_{dry} * 100$$

Samples were repeated three times for the calculation of the statistical average and standard deviation.

Where,  $W_{wet}$  is the weight of the hydrogel after being submersed into DW. However,  $W_{dry}$  is the weight of dry samples before immersed in water.

## **2.5 In vitro Cytotoxicity Assay**

### **2.5.1 MTT Assay**

MTT colorimetric assay was used to analyze cell metabolic activity of GelMA hydrogels and Nanocomposite Hydrogels. Specimens were exposed to UV light for 2 min for sterilization and inserted in 24 well plates. Then 500  $\mu$ l of fibroblast, keratinocytes and endothelial cells suspension at a density of  $5 \times 10^3$  cells were seeded on the surface of the hydrogel. The culture medium was changed every day. At predetermined times, 50  $\mu$ l of 3-(4,5-Dimethyl-2-thiazolyl)-2,5-diphenyl-2H-tetrazolium bromide (MTT) solution were added to each well and kept in an incubator for 4 hours. The supernatant was then removed carefully and 200  $\mu$ l of DMSO (dimethyl sulfoxide) solution was added to dissolve the formazan crystals. 30  $\mu$ l of the solution was transferred into 96 well plates and absorbance were read at 570 nm. For each hydrogel samples, five parallels were averaged.

### **2.5.2 Live/Dead Cell Assay**

The cytotoxicity of GelMA hydrogel and nanocomposite Hydrogels (NCH) on fibroblast, keratinocytes and endothelial cells was investigated using Live/Dead cell imaging kit (488/570, molecular probes, life technologies corp., CA, USA). Cells were

cultured in DMEM medium in 24 well plates for 1 day. The specimens were then added in each well after changing the medium and kept in an incubator for another 24 hours. Following the manufacturer protocols, cells were then stained with Live/Dead cell imaging kit (488/570) (Invitrogen). Images were taken using an Olympus automated fluorescent microscope.

## ***2.6 Cell Migration***

fibroblast, Keratinocytes and endothelial cells were seeded in 24 well plates in DMEM medium. The medium was changed after 24 hours and allowed to incubate for 90% confluency. Using a pipette tip of 10  $\mu$ l, a scratch was made and the cells were washed with PBS to remove died cells. GelMA hydrogels and nanocomposite GelMA hydrogels of 1 wt %, 2 wt%, and 4 wt% was added with the cells and incubated for 24 hours. Using an Olympus microscope, a 4X magnification time-dependent bright field images were taken. The % of wound healing was measured using Imag J software.

## ***2.7 In vivo Model***

### ***2.7.1 CEA Assay***

For the investigation of vascular sprouting, the CEA assay or egg yolk assay is a standard in vivo angiogenesis assay. Fertilized chicken eggs were purchased from Arab Qatari Poultry pharm of Qatar and incubated for 4 days before experiments at a temperature of 37 <sup>0</sup>C with a relative air humidity of 65%. One hour before experiments, a hole of approximately 3mm diameter was made on the egg-shell and covered with a Parafilm to prevent dehydration. The eggs were then kept in the incubator at the static position for one hour. A window was carefully created on the top of the egg shell to provide access to the chorioallantoic membrane. Sterile samples of GelMA hydrogel and nanocomposite hydrogels of 50  $\mu$ l volume were deposited on the chorioallantoic

membrane. The eggs were kept in the incubator for 24 hours in a static position. The eggs were then observed for angiogenesis and photographs were then taken using a stereo microscope as shown in figure.

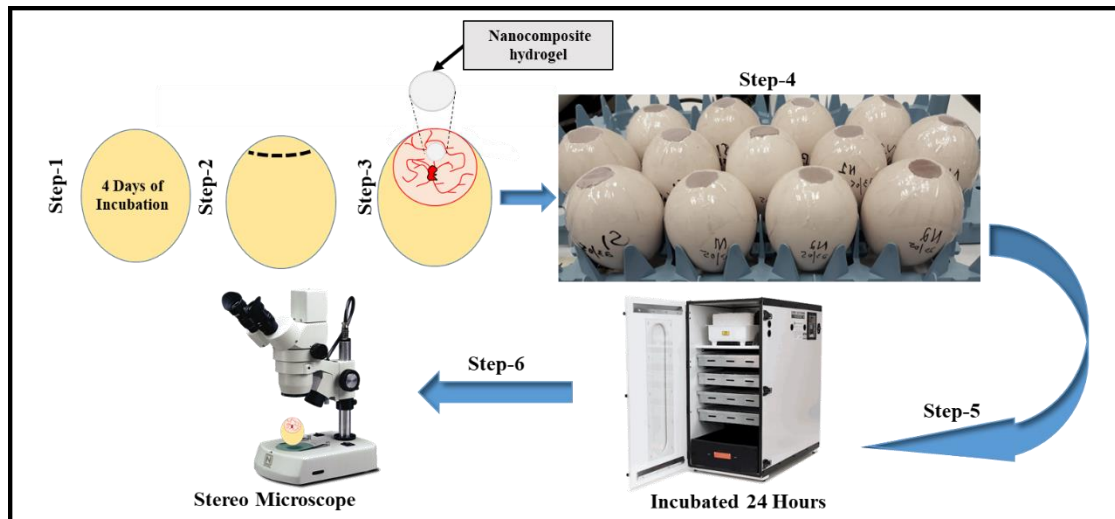


Figure 6: Steps of *in vivo* chicken embryo angiogenesis assay (CEA).

## CHAPTER 3: RESULTS AND DISCUSSION

### 3.1 Results of Physical Characterizations of the Samples

#### 3.1.1 Transmission Electron Microscopic (TEM) images of rGO

The high magnification images of rGO were obtained using transmission electron microscopy as shown in Figure . The TEM images of graphene oxide nanoparticles indicates the amorphous structure (Fig. 3A and 3B). In addition, the average size of individual particle of rGO used in this study was 40 nm.

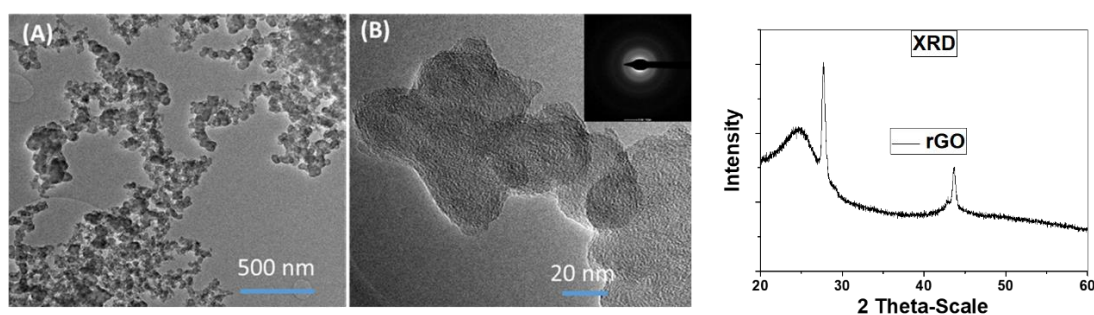


Figure 7: TEM image of rGO structures at 43000X magnification (A) and 400000X magnification (B).

#### 3.1.2 Results of X-Ray Diffraction Analysis

The XRD analysis of the prepared nanocomposite hydrogels was performed to determine the presence of rGO in GelMA hydrogel networks. The XRD pattern of GelMA hydrogel, rGO nanoparticles, 1 wt% rGO loaded GelMA hydrogel (GrG1) and 2 wt% rGO loaded GelMA hydrogel (GrG2) is given in Figure 8. Pure hydrogel samples did not exhibit any sharp peaks in the XRD patterns, with only a broad peak at  $2\theta = 32^\circ$  attributed to the polymer networks as reported in the study of Lei Zhou et al [83]. In the case of rGO, two peaks were observed. These two diffraction peaks in the XRD patterns of rGO, at an angle  $2\theta = 34^\circ$  &  $2\theta = 44^\circ$  can be ascribed to Bragg reflections through (002) & (100) planes as reported in earlier study [84]. The peaks of both GrG1 & GrG2 hydrogels are shifted significantly higher  $2\theta$  values and the XRD showed a strong peak

at  $2\theta = 32^\circ$  &  $2\theta = 46^\circ$ , which was absent in GelMA hydrogel and rGO nanoparticle's pattern as expected.

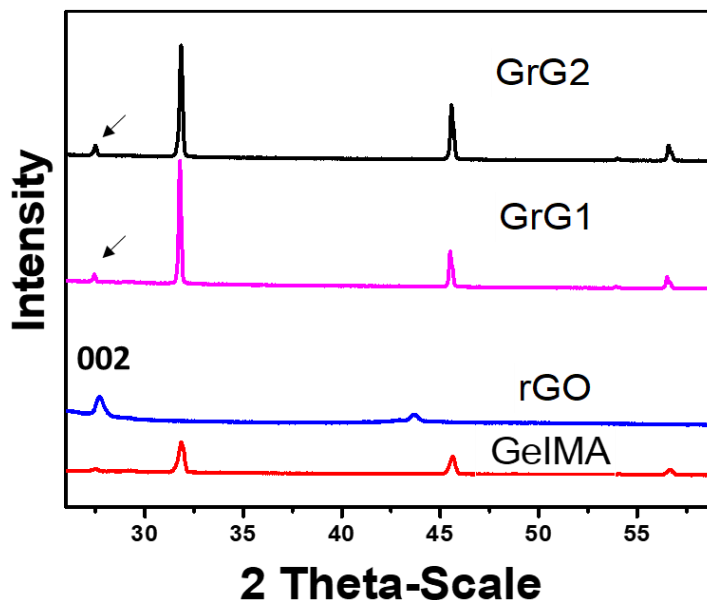


Figure 8: XRD patterns of pure GelMA hydrogel, rGO nanostructures, 1 wt% rGO loaded GelMA hydrogel (GrG1), 2 wt% rGO loaded GelMA hydrogel (GrG2) respectively. The result shows successful incorporation of rGO in GelMA hydrogels.

### 3.1.3 Results of Fourier-Transform Infrared spectroscopy (FTIR)

The presence of rGO is further confirmed by FTIR analysis as shown in Figure 9. The peaks of rGO at wavenumbers of 1589, 1229, 1163, and 846  $\text{cm}^{-1}$  can be seen in the spectra of 2% rGO loaded GelMA hydrogel. However, at less concentration of rGO (0.5%), there was no significant change in the peaks, which might be due to the absence of rGO on the surface of GelMA hydrogel at smaller concentration. However at higher concentration (For eg. 2%), agglomerated forms of rGO might have been exposed at the surface of GelMA and was detected by IR analysis.

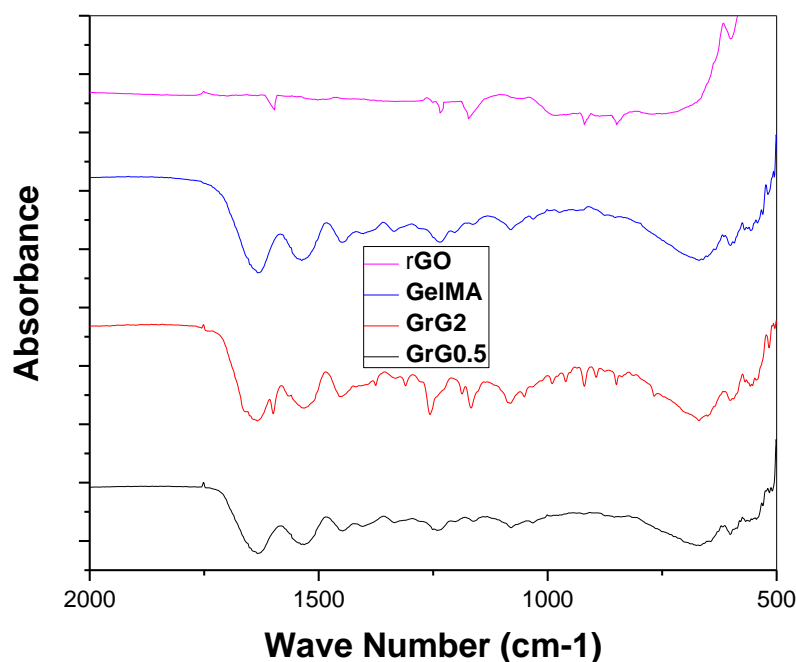


Figure 9: Fourier-transform infrared spectra (FTIR) of rGO, GelMA hydrogel, 2% GO loaded GelMA hydrogel (GrG2) and 0.5 rGO loaded GelMA hydrogel (GrG0.5).

### 3.1.4 Scanning Electron Microscopic images of prepared hydrogels

The surface morphology of rGO incorporated GelMA hydrogel obtained by Scanning Electron Microscopy (SEM) displayed enormous porous structure both on the surface and in the inner regions of the hydrogels. Figure 10 (A) is the representative images showing the surface morphology of GelMA hydrogel. Whereas, Figure 10B and 10C shows the cross-sectional images of GelMA hydrogel. Since rGO doesn't interact covalently GelMA hydrogel, the internal structure and pore size of GelMA hydrogel didn't appear to be significantly affected by the addition of rGO nanostructures. The porous nature of the hydrogels allowed the nanoparticles to penetrate in the hydrogel. The presence of rGO has further confirmed by XRD analysis. Furthermore, the average pore size of GelMA hydrogel is 50  $\mu\text{m}$ , as shown in cross-sectional images of figure 10B and 10C.

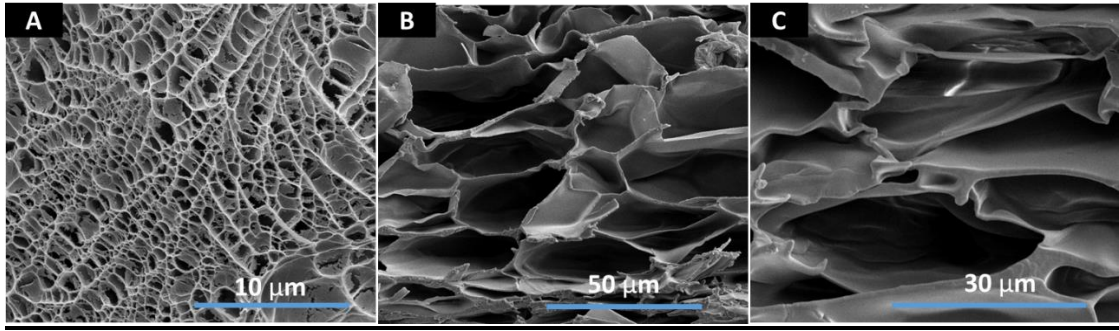


Figure 10: SEM micrograph at 10000X magnification of the surface of (A) GelMA hydrogel, (B) Cross-sectional image of GelMA hydrogel at 5000X, & (C) Cross sectional image of GelMA hydrogel at 2500X magnification.

### ***3.1.5. Results of Degradation of Hydrogels***

Biodegradability of hydrogel has a significant role in wound healing. A porous biodegradable material can provide sufficient space for tissue ingrowth and facilitate tissue repair when implanted into the body or during wound healing [86]. In general, by hydrolysis and enzymolysis, gelatin can be degraded into aminophenol and then absorbed by metabolism and the remaining parts will be excreted from the body, which avoids the accumulation of toxic by-products. In this study, the degradation of GelMA hydrogels and Nanocomposite Hydrogels (NCH) were observed at 37 °C. Unlike the unmodified gelatin, which dissolves within few hours in PBS and loses its three-dimensional structure in most cases, gelatin cross-linked by MA could significantly enhance the stability of gelatin in PBS and maintain its three-dimensional structure at least for 28 days, as shown in Figure 11. This also fulfills the requirement of wound healing and some tissue engineering applications. Moreover, the incorporation of rGO nanoparticles in GelMA hydrogel has enhanced the hydrogel film by decreasing the degradation rate of the hydrogel, as shown in Figure 11.

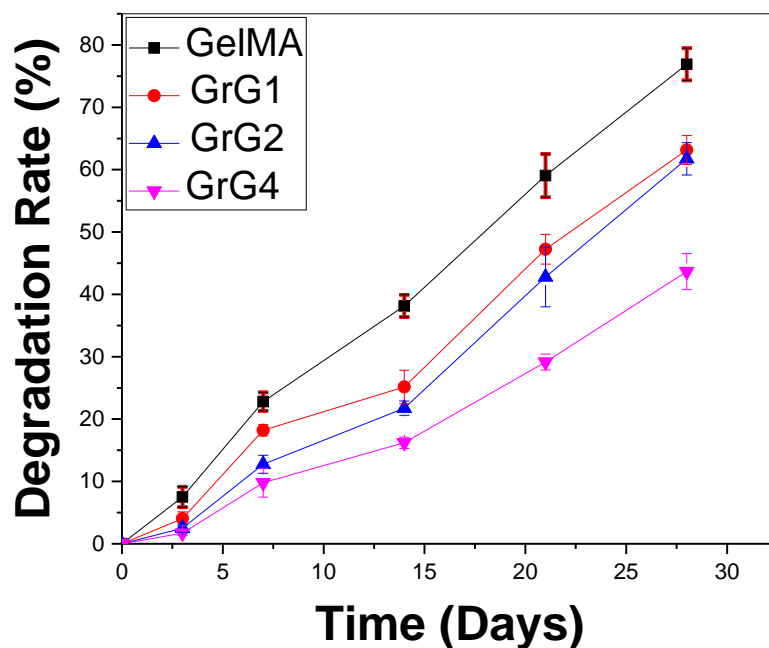


Figure 11: Degradation curve of rGO/GelMA hydrogel films with time. Error bars represent the SD of measurements performed on at least 5 specimens. Result depicts that, gelatin crosslinked by MA could significantly enhance the stability of gelatin in PBS and maintain its three-dimensional structure in PBS at least for 28 days, which fulfill the requirement of wound healing and some tissue engineering applications. Also, the incorporation of rGO nanoparticles in GelMA hydrogel decreased the degradation rate of the hydrogel.

### 3.1.6 Swelling of Prepared Hydrogels

The swelling percentage of GelMA hydrogel and nanocomposite GelMA hydrogel has significantly increased within the first 15 minutes of immersion in PBS as shown in Figure 12. However, the differences in swelling percentage within GelMA hydrogel and nanocomposite GelMA hydrogel was not significant. Swelling equilibrium was reached within 30 minutes. The incorporation of rGO has not affected the swelling behavior of the hydrogel.

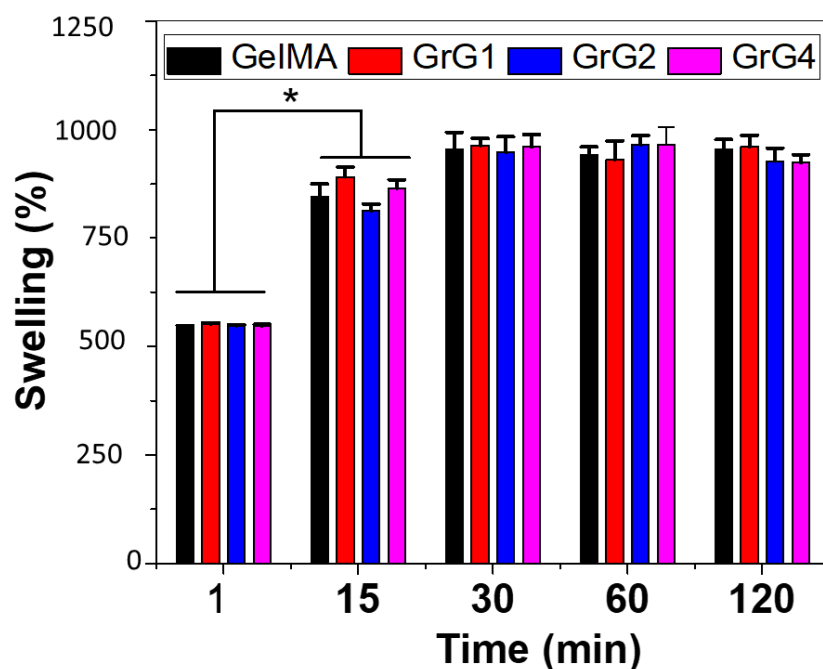


Figure 12: The swelling percentage of GelMA hydrogel and nanocomposite GelMA hydrogel after 0, 15, 30, 60 and 120 minutes respectively.

### 3.1.8 Results of Dynamic Mechanical Analysis (DMA)

The dynamic mechanical analysis (DMA) is carried out to observe the difference in storage ( $G''$ ) and loss modulus ( $G'$ ) after the incorporation of rGO in GelMA hydrogel. The amplitude and frequency sweep test (Figure 13A and 13B) revealed that the incorporation of rGO has enhanced the viscoelastic properties of GelMA hydrogel. The ranges of storage and loss moduli for both amplitude and frequency sweep test was higher for 2% GO loaded GelMA hydrogel than neat GelMA hydrogel.

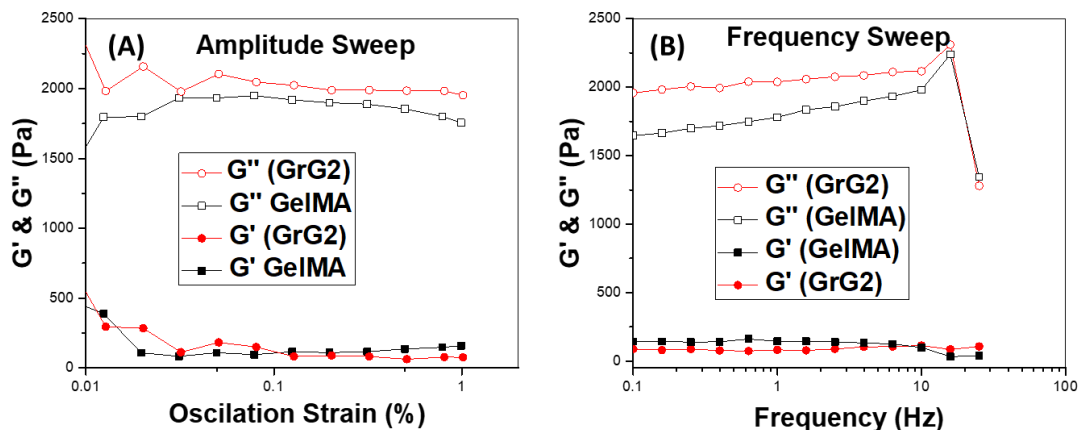


Figure 13: The storage and loss modulus ranges in amplitude sweep test (A) and frequency sweep test (B) of GelMA hydrogel and 2% rGO loaded GelMA hydrogel (GrG2).

## 3.2 Results of *in vitro* Cytotoxicity assays

### 3.2.1 Live/Dead Assay

The nanocomposite hydrogel has proven to potentially improve cell viability and proliferation, while studies also have reported that the nanomaterials have a serious concern of cytotoxicity. In order to understand the biocompatibility of the hydrogel and visualize the distribution of live and dead cells after 24 hours of incubations, the Live/Dead cell assay on three different cell lines (fibroblast, endothelial & keratinocytes) was performed. The cytotoxicity on culture media (control), GelMA hydrogel and nanocomposite hydrogel containing 1 wt% (GrG1), 2 wt% (GrG2), and 4 wt% (GrG4) of rGO nanoparticles were evaluated by using three cell lines as shown in Figure 14, 15 & 16. The cells remained alive and no significant cytotoxic effect was observed in all the studied samples up to 2 wt% concentration of rGO. However, at higher concentration of rGO (4 wt%) some dead cells were observed as shown in the middle column (denoted as dead cells) in figures. Overall results depict that the reduced rGO upto 2% concentration in GelMA hydrogel has almost no toxic effect on the cells. However, at higher concentration, it can be slightly toxic.

In a recent study, rGO has reported being toxic to the cells when administered in the form of a solution at concentrations above  $100 \text{ nm ml}^{-1}$  [52]. In this study, with the incorporation in GelMA hydrogel, rGO nanoparticles have shown no toxic effect at a concentration higher than its cytotoxic concentration in free solution. The reason could be the slow release of rGO nanoparticles from the hydrogel, which enables them to present at a concentration lower than the cytotoxic level to the cells.

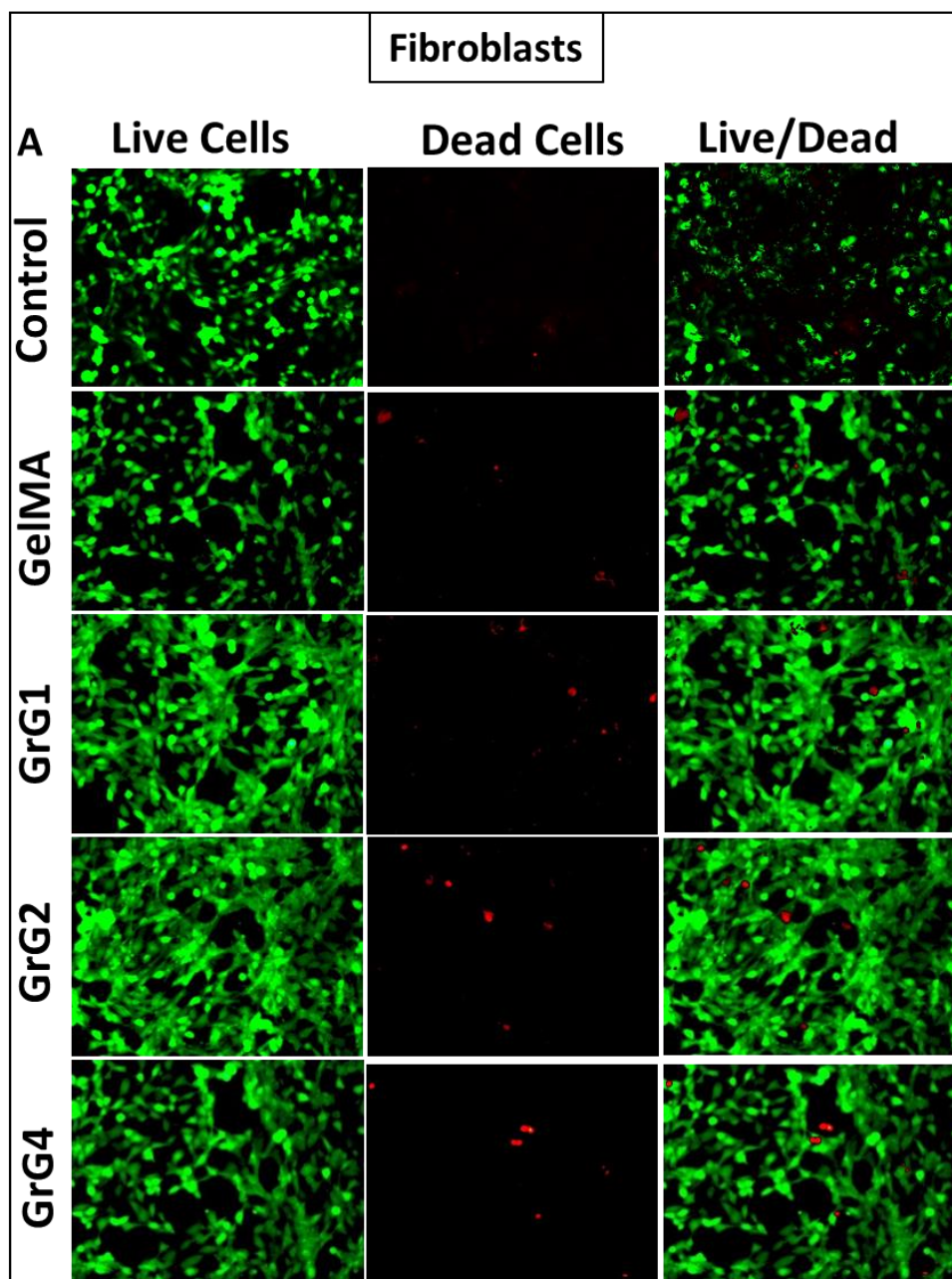


Figure 14: Cell viability (Live/Dead cell assay) on fibroblast for control, pure GelMA hydrogel, 1% rGO loaded GelMA hydrogel (GrG1), 2% rGO loaded GelMA hydrogel (GrG2) and 4% rGO loaded GelMA hydrogel (GrG4) respectively. Green channel depicts live cells, while red channels depict compromised dead cells.

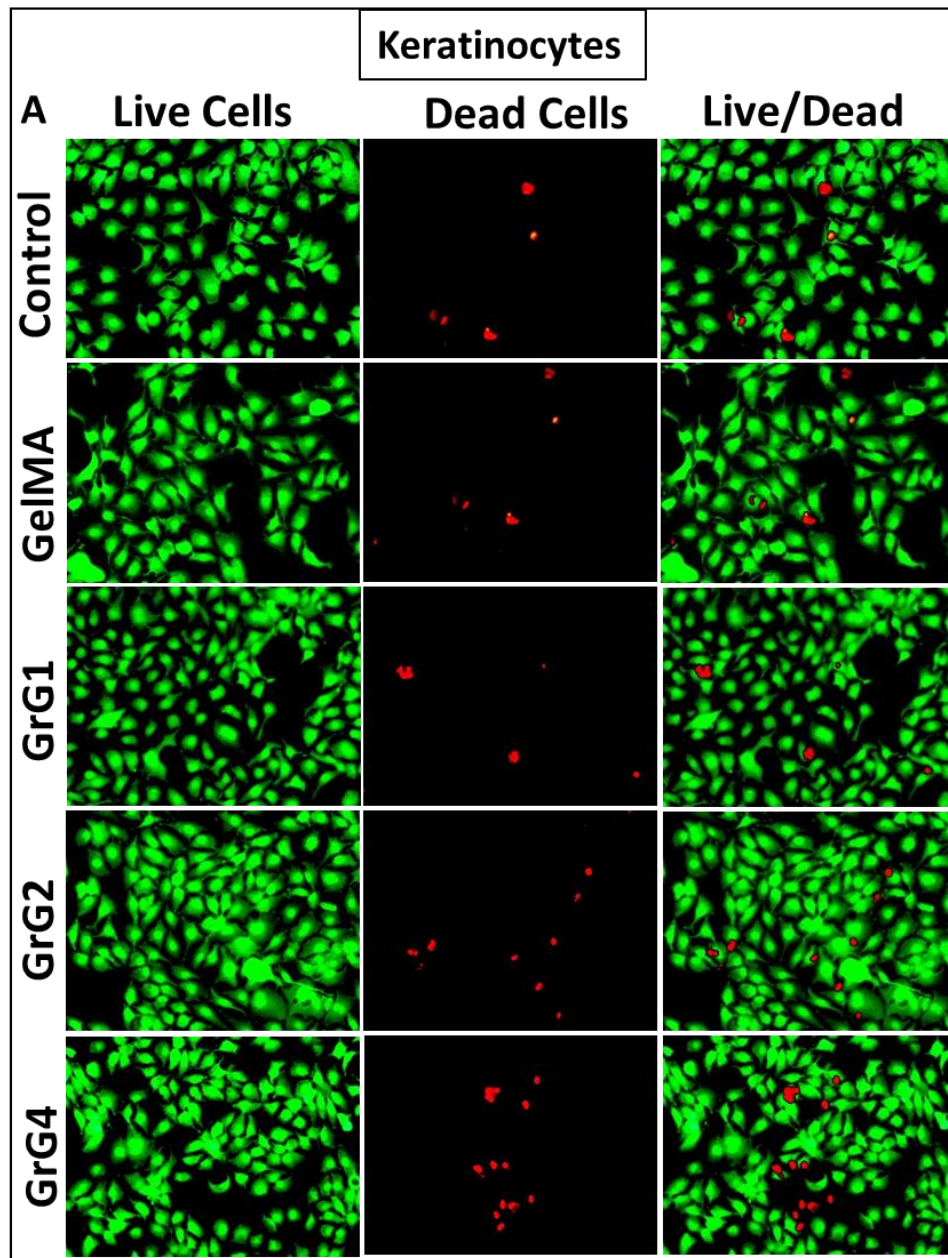


Figure 15: Cell viability (Live/Dead cell assay) on Keratinocytes for control, pure GelMA hydrogel, 1% rGO loaded GelMA hydrogel (GrG1), 2% rGO loaded GelMA hydrogel (GrG2) and 4% rGO loaded GelMA hydrogel (GrG4) respectively. Green channel depicts live cells, while red channels depict compromised dead cells.

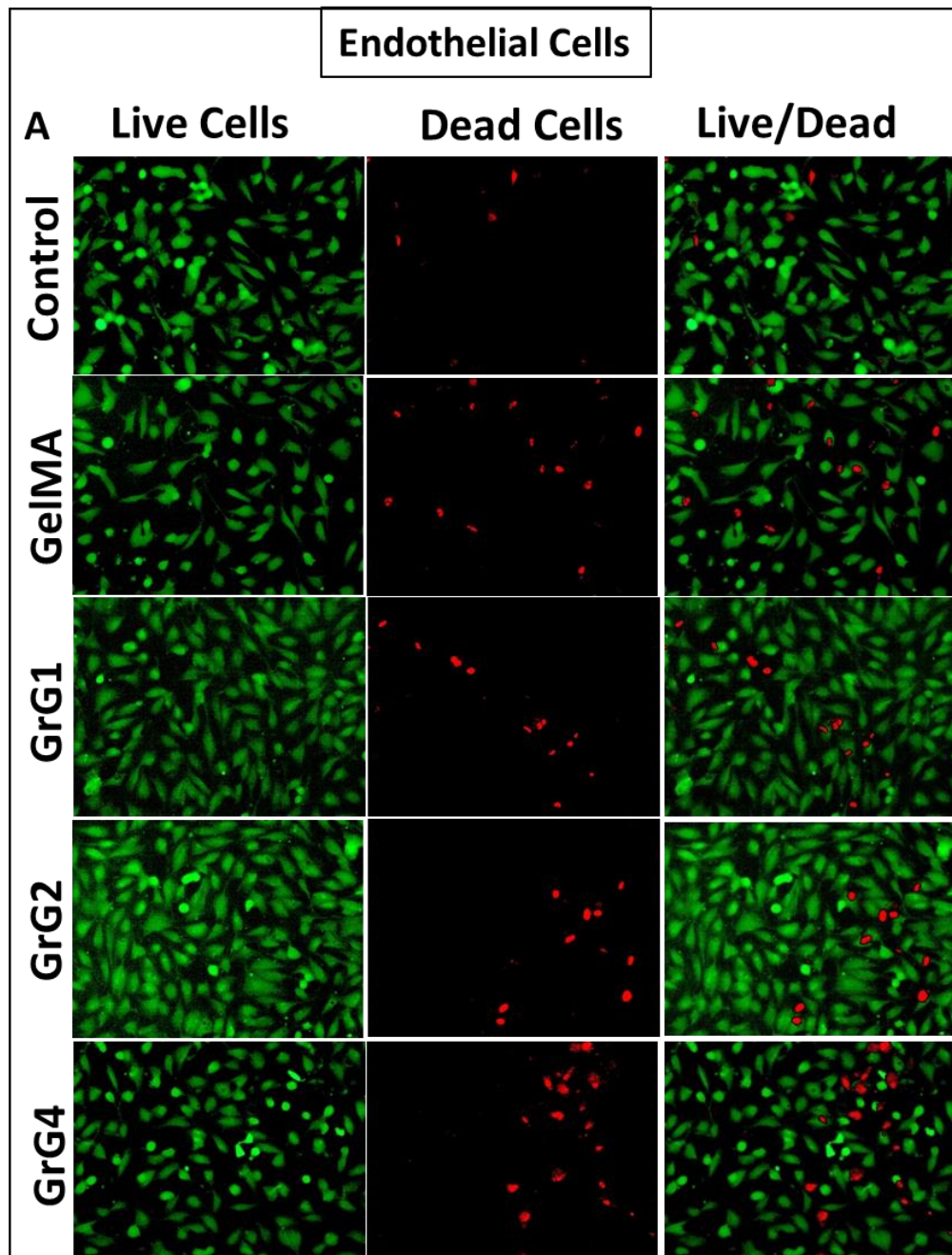


Figure 16: Cell viability (Live/Dead cell assay) on endothelial cells for control, pure GelMA hydrogel, 1% rGO loaded GelMA hydrogel (GrG1), 2% rGO loaded GelMA hydrogel (GrG2) and 4% rGO loaded GelMA hydrogel (GrG4) respectively. Green channel depicts live cells, while red channels depict compromised dead cells.

### 3.2.2 MTT Cell Viability Assay

The MTT cell viability assay was implemented to investigate the cell metabolic activity of fibroblast, endothelial and keratinocytes cells on GelMA hydrogel and nanocomposite GelMA hydrogels quantitatively, after 1, 3 and 5 days in culture. A

significant effect of rGO ( $* = p < 0.05$ ) was observed on cell metabolic activity after 1 day and shown in Figure 17, 18, & 19. However, after 3 days of treatment, the difference is not very significant. These results revealed all three cell lines had an increased metabolic activity on rGO loaded GelMA hydrogel up to 2% (GrG2) concentration compared to the control and pure GelMA hydrogel. Particularly, after 1 day and 5 days in culture, MTT assay had shown the highest cellular metabolic activity of fibroblast for 2% rGO loaded GelMA hydrogel (GrG2). However, increasing the concentration of rGO reduced the cells metabolic activity.

Generally, the MTT assay is used to measure the viability of cells in terms of the reduction of MTT reagent by mitochondrial enzymes. Therefore, the higher metabolic measurement from the assay presents more cell attachment to the hydrogel surface and the subsequent proliferation. The slow release of rGO from the degrading hydrogels which could have helped in cell proliferation could be the reason for the increased proliferation of the cells.

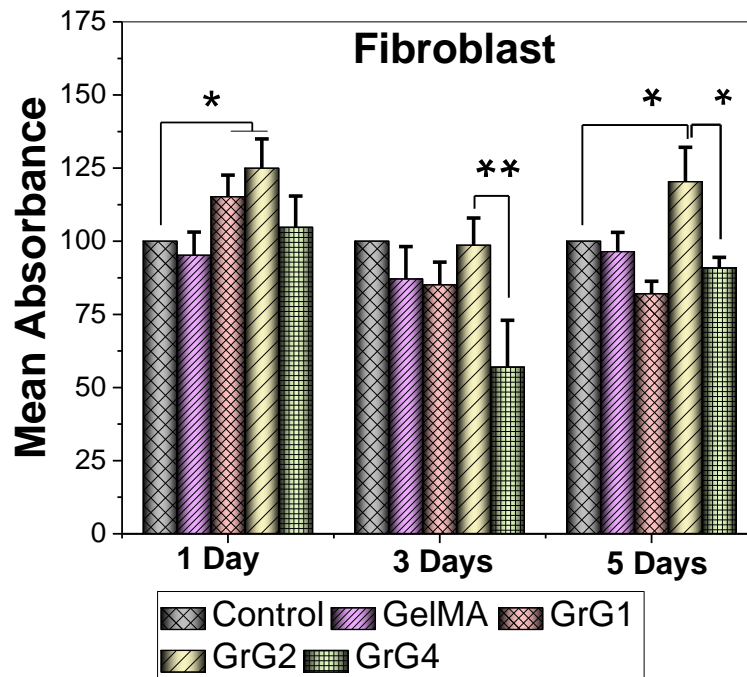


Figure 17: Results of MTT assay using fibroblast cells for 1 day, 3 days and 5 days. The incorporation of rGO nanoparticles (GrG1 & GrG2) has significantly increased the cell metabolic activity after 1 day and 5 days of incubation. However, the cell metabolic activity has reduced significantly at higher concentration (GrG4) after 3 days and 5 days of incubations. Result depicts that the rGO up to 2% concentration in GelMA hydrogel has almost no toxic effect on biocompatibility, however, at higher concentration it can be slightly cytotoxic to fibroblasts.

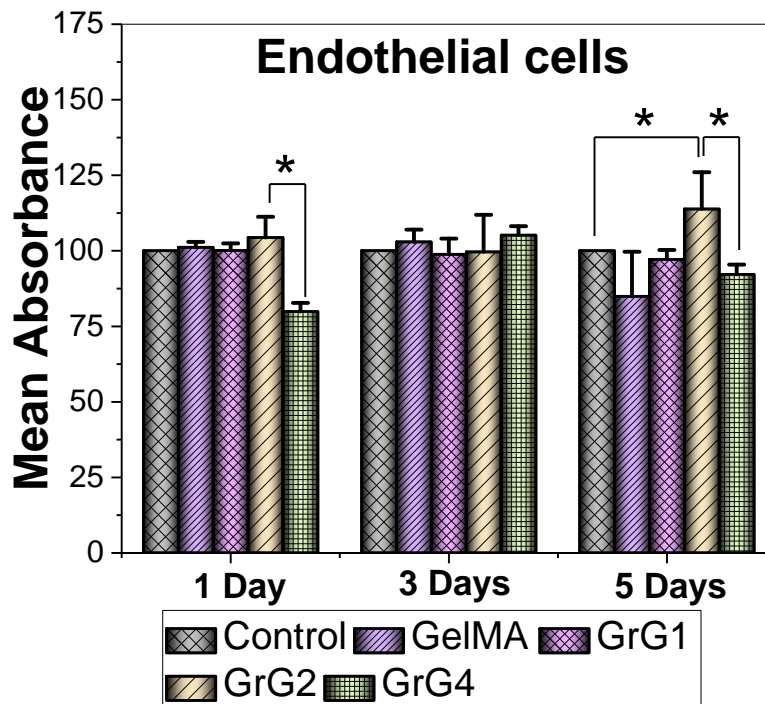


Figure 18: Results of MTT assay using endothelial cells for 1 day, 3 days and 5 days. Result depicts that the rGO up to 2% concentration in GelMA hydrogel has almost no toxic effect on biocompatibility, however, at higher concentration it can be slightly cytotoxic to endothelial cells.

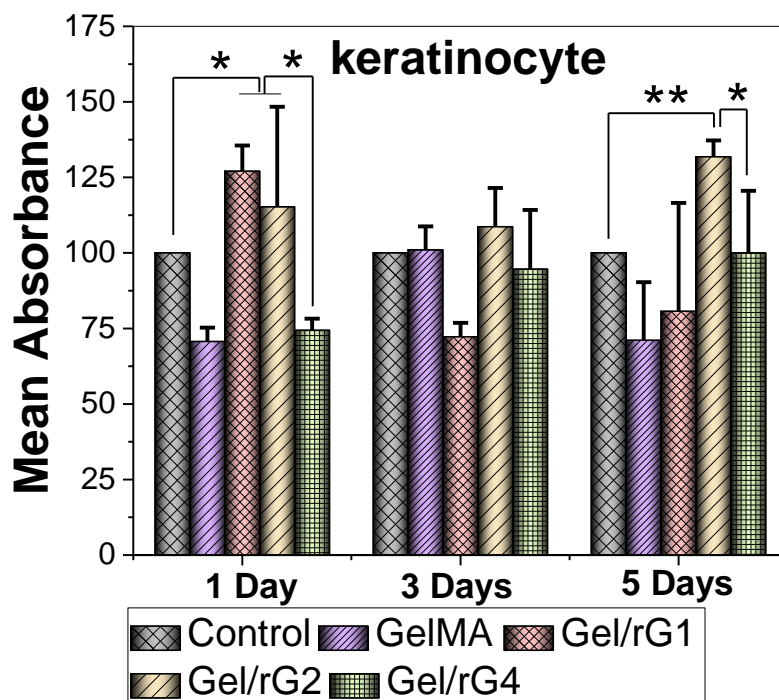


Figure 19: Results of MTT assay using keratinocyte cells for 1 day, 3 days and 5 days. A significant increment in cell metabolic activity (\*\* =  $P < 0.01$ ) was observed between control and GrG2. Moreover, the increment of both GrG1 and GrG2 is significant (\* =  $P < 0.05$ ) after 1 day of incubation. However, at higher concentration of rGO (GrG4) a significant reduction in cell metabolic activity after 1 day and 5 days of incubations. Result depicts that the rGO up to 2% concentration in GelMA hydrogel has almost no toxic effect on biocompatibility, however, at higher concentration it can be toxic to keratinocytes.

### 3.2.3 Results of *in vitro* Wound Healing Assay

Cell migration is one of the key steps in the wound healing process [87]. Recently rGO has been reported to enhance the migration of endothelial cells at a concentration of 1-50  $\text{ng ml}^{-1}$  indicating their pro-angiogenic nature [52]. In this study, a time-dependent experiment (0-24 hours) was carried out in the presence of different concentration of rGO with GelMA hydrogel in order to check the migration of fibroblast, keratinocytes and endothelial cells as shown in Figure 20, 21 & 22. The results depict that, GelMA hydrogel incorporated 2 wt% rGO nanoparticles (GrG2) induced the *in vitro* wound closure compared to control untreated cells and 1 wt% rGO (GrG1) treated cells (Figure

20,21, & 22) in all three cell lines. However, rGO has not shown wound *in vitro* healing property (wound closure) at higher concentration (4%) compared to untreated control cells. Particularly, fibroblast has shown maximum cell migration (85%) due to its less passage number. However, both endothelial and HaCat cells have shown maximum cell migration percentage at 2 wt% rGO loaded GelMA hydrogel (GrG2) samples. In Figure 20(B), 21(B), & 22(B) the extent of wound healing was quantified and presented as histograms. The results altogether demonstrated that the cells at 2 wt% concentration of rGO could enhance the migration of the cells which indicates their wound healing property, while at higher concentration it could inhibit wound contraction.

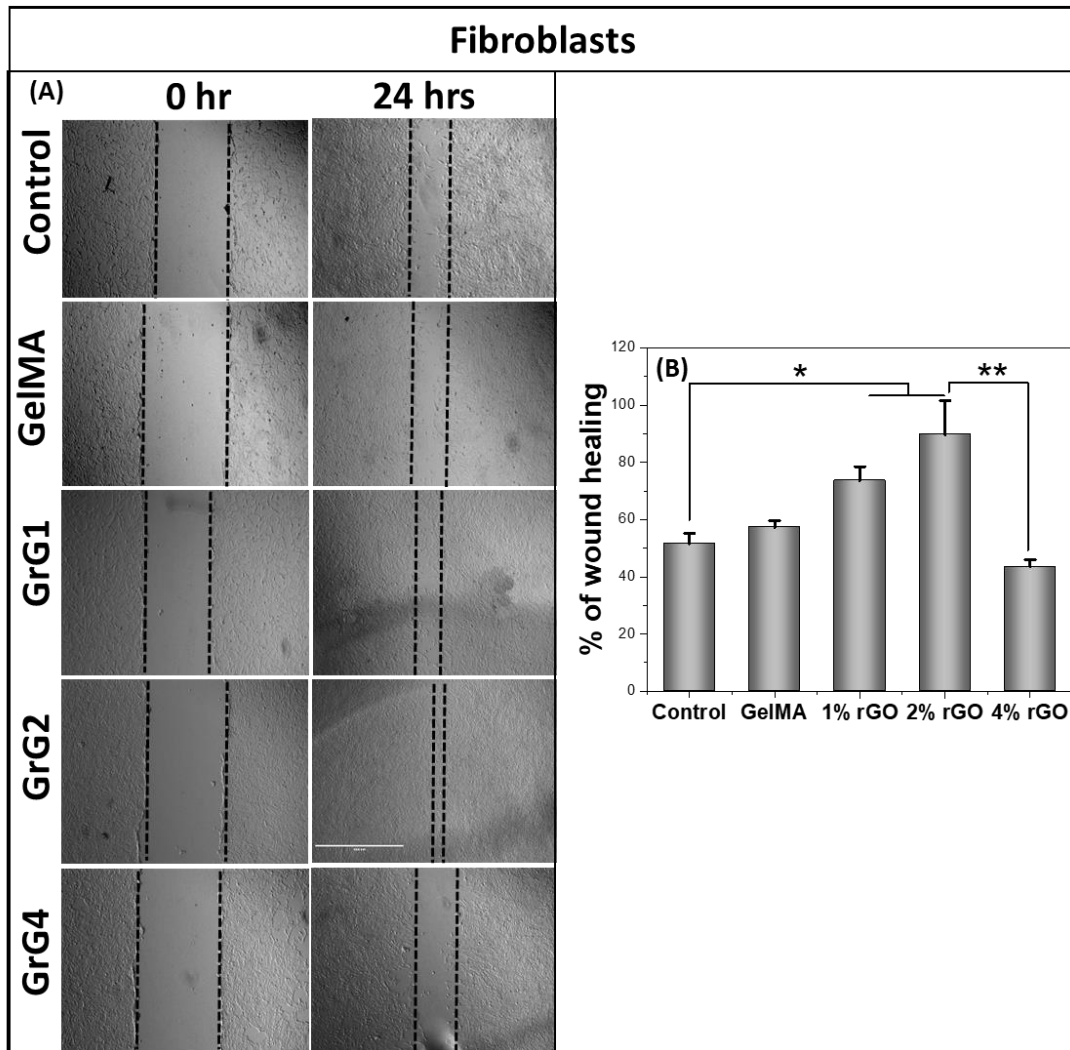


Figure 20: Results of *in vitro* wound healing scratch assay using fibroblast cells for control, GelMA hydrogel, 1% rGO loaded GelMA hydrogel (GrG1), 2% rGO loaded GelMA hydrogel (GrG2), & 4% rGO loaded GelMA hydrogel (GrG4) treatment groups. Percentage of wound healing was measured and presented as histograms using ImageJ software. A significant wound healing ( $* = P < 0.05$ ) was observed with the incorporation of 1 wt% and 2wt% rGO (GrG1, GrG2) in GelMA hydrogel. However, at higher concentration there was a significant reduction in cell migration ( $** = P < 0.01$ ).

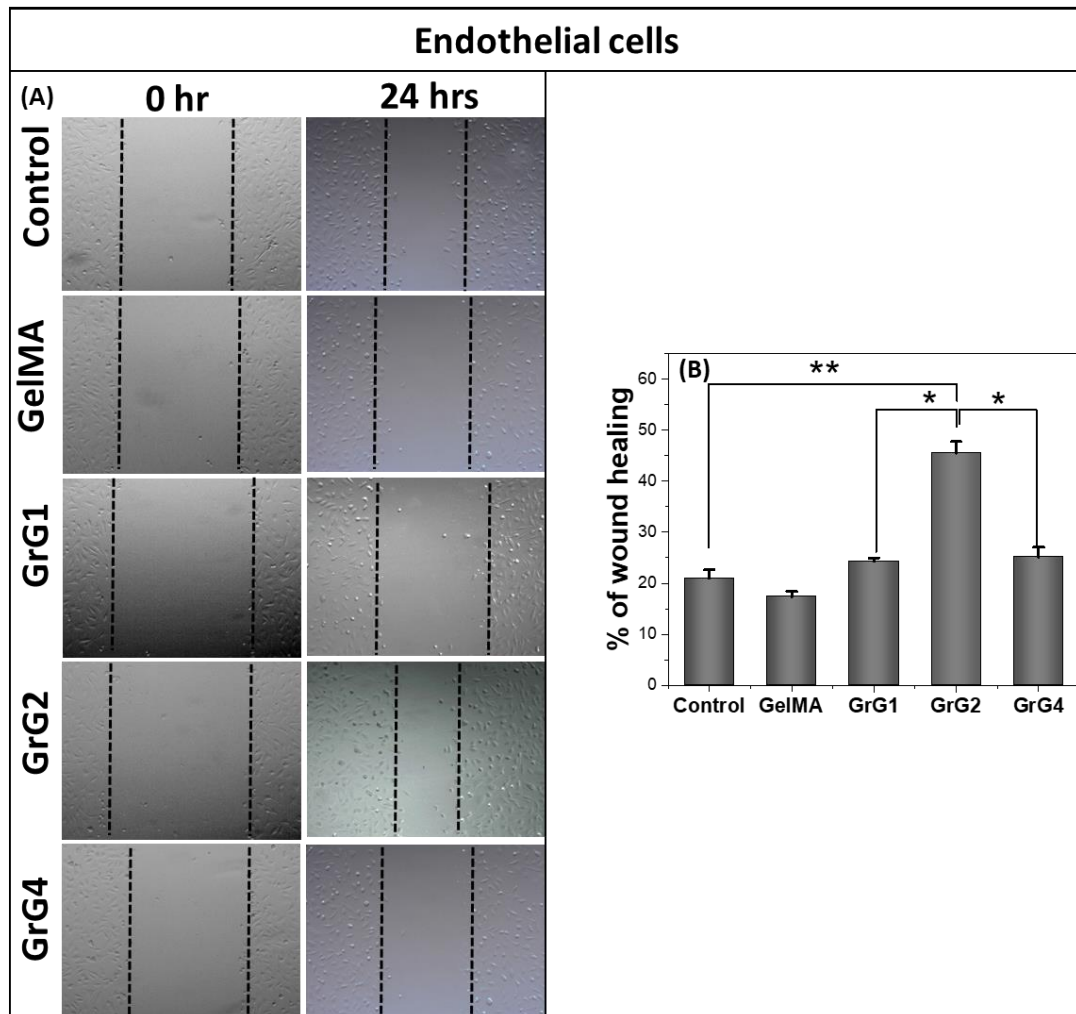


Figure 21: Results of *in vitro* wound healing scratch assay using endothelial cells for control, GelMA hydrogel, 1% rGO loaded GelMA hydrogel (GrG1), 2% rGO loaded GelMA hydrogel (GrG2), & 4% rGO loaded GelMA hydrogel (GrG4) treatment, groups. (B) Percentage of wound healing was measured and presented on histogram using ImageJ software (Figure 17B). The incorporation of rGO up to 2wt% concentration has shown highest percentage of cell migration compared to the control, GrG1 and GrG4 (\* =  $P < 0.05$ , \*\* =  $P < 0.01$ ).

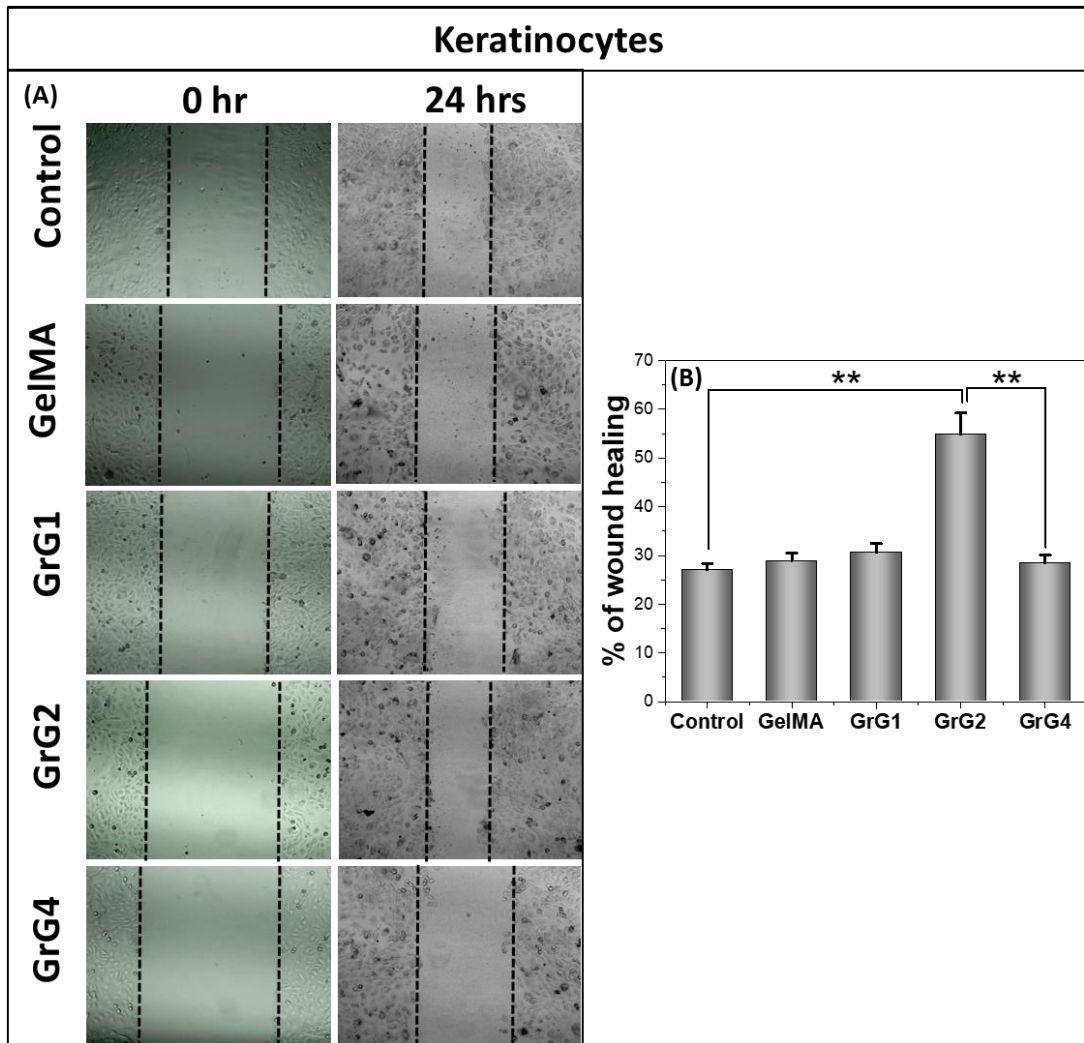


Figure 22: Results of *in vitro* wound healing scratch assay using Keratinocytes for control, GelMA hydrogel, 1% rGO loaded GelMA hydrogel (GrG1), 2% rGO loaded GelMA hydrogel (GrG2), & 4% rGO loaded GelMA hydrogel (GrG4) treatment, groups. (B) Percentage of wound healing was measured and presented on histogram using ImageJ software (Figure 18B). Significant wound healing was observed at 2% concentration of rGO in GelMA hydrogel (GrG2). The results altogether demonstrated that the cells at 2 wt% concentration of rGO could enhance the migration of the cells, while at higher concentration it could be toxic (\* =  $P < 0.01$ ).

### 3.2.4 Results of Chicken Embryo Angiogenesis (CEA) Study

In order to evaluate the angiogenic potential of the developed rGO loaded GelMA hydrogels, the chicken embryo angiogenesis (CEA) assay was used as a standard test. It was carried out to investigate the ability of the synthesized hydrogel to induce blood vessel formation (angiogenesis). The results of CEA assay are shown in Figure 23(A) where the control, GelMA hydrogel, GelMA hydrogel containing 1 wt% (GrG1) and 2

wt% (GrG2) rGO, respectively. A significant increase in vascular sprouting was observed in GelMA hydrogel incorporated with 1 wt% (GrG1), and 2 wt% (GrG1) rGO compared with the control (cell culture plate). The highest number of blood vessels with the highly branched capillary network (1.7 times higher than the control) can be observed at 1% rGO loaded GelMA hydrogel (GrG1). The 2% rGO loaded GelMA hydrogel (GrG2) showed 1.6 and 1.7 times higher length and thickness of blood vessels respectively than the control. The increase in thickness is an indication of nascent blood vessels maturation and is possibly an outcome of arteriogenesis. Thus, the obtained results suggested that the hydrogel has successfully enhanced both angiogenesis and arteriogenesis. The pure GelMA hydrogel didn't show any significant angiogenic activity when compared with the control. Whereas, the control samples didn't considerably increase the angiogenesis. Thus, with the increase of rGO concentration up to 2 wt% the angiogenic potential of the GelMA hydrogel increased. A number of branching points were counted, change in length and thickness of blood vessels were measured using ImageJ software after 24 hours of incubation and presented in the histogram as shown in Figure 23B, 23C and 23D respectively.

As found in a recent study, rGO has the ability to increase the concentration of intracellular reactive oxygen species [52]. And eventually, the increase in the concentration of reactive oxygen species triggers the biomechanical machinery which is responsible for both angiogenesis and arteriogenesis [52]. However, in order to understand the molecular mechanism behind our observation, further studies need to be performed using animal models.

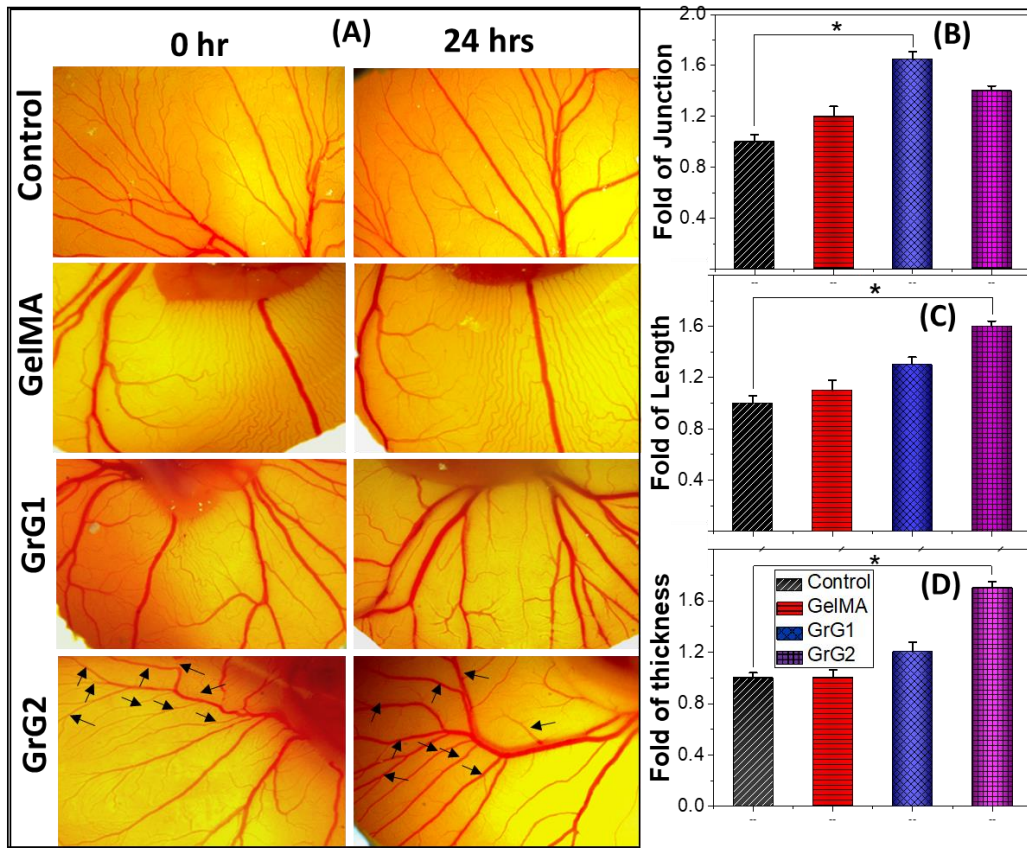


Figure 23: (A) *In vivo* CEA assay of control, in the presence of the GelMA hydrogel, 1 wt% rGO loaded GelMA hydrogel (GrG1), and 2 wt% rGO loaded GelMA hydrogel (GrG2). An increase of matured blood vessel formation (marked by black arrows) was observed in chicken embryo treated with GelMA hydrogel with 2 wt% rGO (GrG2). Angiogenic parameters such as blood vessel junction, length, and thickness were quantified and presented as a histogram (B, C & D respectively). Statistical significance was calculated by using *t*-test. Data was considered statistically significant at  $p < 0.05$ .

## CHAPTER 4: CONCLUSION

### 4.1 Conclusions

The ability of reduced graphene oxide nanoparticles to enhance the intercellular reactive oxygen species concentration was founded in the previous study. This triggers the biomechanical machinery which is responsible for both angiogenesis and arteriogenesis. In this study, we have successfully synthesized rGO incorporated GelMA hydrogel pro-angiogenic wound healing patch by UV crosslinking. Our prepared GelMA hydrogel displayed highly porous structures. The SEM images displayed surface and cross-sectional views of GelMA hydrogel. The average pore sizes observed by SEM images are 50  $\mu\text{m}$ . The TEM images confirmed the amorphous structure and 20 nm average size of reduced graphene oxide nanoparticles. The XRD analysis confirmed the nanoparticle formation in GelMA hydrogel. A certain peak shift was observed in the XRD pattern due to a non-covalent bonding of functional groups of rGO with the hydrogel. The incorporation of rGO nanoparticles in GelMA hydrogel is further confirmed by Fourier-transform infrared spectroscopy (FTIR). The degradability study has shown that gelatin crosslinked by MA could significantly enhance the stability of gelatin in PBS and maintain its three-dimensional structure in PBS at least for 28 days, which fulfill the requirement of wound healing and some tissue engineering applications. The swelling behavior of GelMA hydrogel has shown the excellent hydrophilic property. The thermal gravimetric analysis result has shown the thermal stability of the hydrogel in the vicinity of room temperature which normally varies between 27 and 38  $^{\circ}\text{C}$ . The amplitude and frequency sweep test reveal that the incorporation of rGO has enhanced the viscoelastic properties of GelMA hydrogel. *In vitro* cytotoxicity assay (Live/Dead and MTT assay) has demonstrated the biocompatibility of the hydrogel. The cells remain alive and no significant cytotoxic

effect was observed in all samples up to 2 wt% concentration of rGO. MTT assay has shown the highest cell metabolic activity on all three cell lines particularly after 1 day and 5 days of incubations for 2% rGO loaded GelMA hydrogel. Moreover, our synthesized material exhibited remarkable wound healing potential displaying improved fibroblast, keratinocytes, and endothelial proliferation. In addition, GelMA hydrogel containing 2% rGO nanoparticles produced a large number of blood vessels with a highly branched capillary network in the chick embryo model compared to blank GelMA hydrogel treatment only. However, further studies will have to be performed to understand the molecular mechanism involved in this process beyond our observations.

## **4.2 Further Recommendations**

Reduced graphene oxide loaded GelMA hydrogel could be a promising material for enhanced wound healing of acute and chronic wounds. We strongly believe that our study on rGO/GelMA hydrogel will put forward the insight for the advancement of angiogenic treatment strategies for several diseases where angiogenesis plays a significant role. Moreover, this will also pave the ways in the advancement of different tissue engineering applications by making artificial tissues using GelMA hydrogel. However, further studies are required to understand the molecular mechanism involved in this process beyond our observations.

## REFERENCES

1. Wild, S., et al., *Global prevalence of diabetes: estimates for the year 2000 and projections for 2030*. *Diabetes care*, 2004. **27**(5): p. 1047-1053.
2. Reiber, G.E., et al., *Causal pathways for incident lower-extremity ulcers in patients with diabetes from two settings*. *Diabetes care*, 1999. **22**(1): p. 157-162.
3. Reiber, G.E., E.J. Boyko, and D.G. Smith, *Lower extremity foot ulcers and amputations in diabetes*. *Diabetes in America*, 1995. **2**: p. 409-27.
4. Falanga, V., *Wound healing and its impairment in the diabetic foot*. *The Lancet*, 2005. **366**(9498): p. 1736-1743.
5. Galiano, R.D., et al., *Topical vascular endothelial growth factor accelerates diabetic wound healing through increased angiogenesis and by mobilizing and recruiting bone marrow-derived cells*. *The American journal of pathology*, 2004. **164**(6): p. 1935-1947.
6. Archana, D., J. Dutta, and P. Dutta, *Evaluation of chitosan nano dressing for wound healing: Characterization, in vitro and in vivo studies*. *International journal of biological macromolecules*, 2013. **57**: p. 193-203.
7. Galkowska, H., U. Wojewodzka, and W.L. Olszewski, *Chemokines, cytokines, and growth factors in keratinocytes and dermal endothelial cells in the margin of chronic diabetic foot ulcers*. *Wound Repair and Regeneration*, 2006. **14**(5): p. 558-565.
8. Goren, I., et al., *Severely impaired insulin signaling in chronic wounds of diabetic ob/ob mice: a potential role of tumor necrosis factor- $\alpha$* . *The American journal of pathology*, 2006. **168**(3): p. 765-777.
9. Chao, C.Y. and G.L. Cheing, *Microvascular dysfunction in diabetic foot disease and ulceration*. *Diabetes/metabolism research and reviews*, 2009. **25**(7): p. 604-614.
10. Dinh, T. and A. Veves, *Microcirculation of the diabetic foot*. *Current pharmaceutical design*, 2005. **11**(18): p. 2301-2309.
11. Chen, H., et al., *Quickly promoting angiogenesis by using a DFO-loaded photocrosslinked gelatin hydrogel for diabetic skin regeneration*. *Journal of Materials Chemistry B*, 2016. **4**(21): p. 3770-3781.
12. Dong, Y., et al., *Performance of an in situ formed bioactive hydrogel dressing from a PEG-based hyperbranched multifunctional copolymer*. *Acta biomaterialia*, 2014. **10**(5): p. 2076-2085.
13. Borenstein, J.T., et al., *Functional endothelialized microvascular networks with circular cross-sections in a tissue culture substrate*. *Biomedical microdevices*, 2010. **12**(1): p. 71-79.
14. Sadr, N., et al., *SAM-based cell transfer to photopatterned hydrogels for microengineering vascular-like structures*. *Biomaterials*, 2011. **32**(30): p. 7479-7490.
15. Alajati, A., et al., *Spheroid-based engineering of a human vasculature in mice*. *Nature methods*, 2008. **5**(5): p. 439.
16. Lesman, A., et al., *Transplantation of a tissue-engineered human vascularized cardiac muscle*. *Tissue Engineering Part A*, 2009. **16**(1): p. 115-125.
17. Phelps, E.A., et al., *Bioartificial matrices for therapeutic vascularization*. *Proceedings of the National Academy of Sciences*, 2010. **107**(8): p. 3323-3328.
18. Saik, J.E., et al., *Biomimetic hydrogels with immobilized ephrinA1 for therapeutic angiogenesis*. *Biomacromolecules*, 2011. **12**(7): p. 2715-2722.
19. Leslie-Barbick, J.E., J.J. Moon, and J.L. West, *Covalently-immobilized vascular*

- endothelial growth factor promotes endothelial cell tubulogenesis in poly (ethylene glycol) diacrylate hydrogels.* Journal of Biomaterials Science, Polymer Edition, 2009. **20**(12): p. 1763-1779.
20. Bae, H., et al., *Building vascular networks.* Science translational medicine, 2012. **4**(160): p. 160ps23-160ps23.
  21. Mao, A.S. and D.J. Mooney, *Regenerative medicine: current therapies and future directions.* Proceedings of the National Academy of Sciences, 2015. **112**(47): p. 14452-14459.
  22. Balakrishnan, B., et al., *Evaluation of an in situ forming hydrogel wound dressing based on oxidized alginate and gelatin.* Biomaterials, 2005. **26**(32): p. 6335-6342.
  23. Kennedy, J.F., C.J. Knill, and M. Thorley, *Natural polymers for healing wounds,* in *Recent advances in environmentally compatible polymers.* 2001, Elsevier. p. 97-104.
  24. Boehm, H., R. Setton, and E. Stumpp, *Nomenclature and terminology of graphite intercalation compounds.* 1986, Pergamon.
  25. Geim, A.K., *Graphene: status and prospects.* science, 2009. **324**(5934): p. 1530-1534.
  26. Novoselov, K.S. and A. Geim, *The rise of graphene.* Nat. Mater, 2007. **6**(3): p. 183-191.
  27. Novoselov, K.S., et al., *Electric field effect in atomically thin carbon films.* science, 2004. **306**(5696): p. 666-669.
  28. Zhu, Y., et al., *Graphene and graphene oxide: synthesis, properties, and applications.* Advanced materials, 2010. **22**(35): p. 3906-3924.
  29. Terzopoulou, Z., G. Kyzas, and D. Bikiaris, *Recent advances in nanocomposite materials of graphene derivatives with polysaccharides.* Materials, 2015. **8**(2): p. 652-683.
  30. Huang, Y., et al., *Multi-structural network design and mechanical properties of graphene oxide filled chitosan-based hydrogel nanocomposites.* Materials & Design, 2018. **148**: p. 104-114.
  31. Räder, H.J., et al., *Processing of giant graphene molecules by soft-landing mass spectrometry.* Nature materials, 2006. **5**(4): p. 276.
  32. Wujcik, E.K. and C.N. Monty, *Nanotechnology for implantable sensors: carbon nanotubes and graphene in medicine.* Wiley Interdisciplinary Reviews: Nanomedicine and Nanobiotechnology, 2013. **5**(3): p. 233-249.
  33. Wang, C., et al., *Gold nanoclusters and graphene nanocomposites for drug delivery and imaging of cancer cells.* Angewandte Chemie International Edition, 2011. **50**(49): p. 11644-11648.
  34. Garaj, S., et al., *Graphene as a subnanometre trans-electrode membrane.* Nature, 2010. **467**(7312): p. 190.
  35. Eda, G., G. Fanchini, and M. Chhowalla, *Large-area ultrathin films of reduced graphene oxide as a transparent and flexible electronic material.* Nature nanotechnology, 2008. **3**(5): p. 270.
  36. Pyun, J., *Graphene oxide as catalyst: application of carbon materials beyond nanotechnology.* Angewandte Chemie International Edition, 2011. **50**(1): p. 46-48.
  37. Tang, J., et al., *Graphene oxide–silver nanocomposite as a highly effective antibacterial agent with species-specific mechanisms.* ACS applied materials & interfaces, 2013. **5**(9): p. 3867-3874.
  38. Pan, Y., et al., *Water-soluble poly (N-isopropylacrylamide)–graphene sheets*

- synthesized via click chemistry for drug delivery*. *Advanced Functional Materials*, 2011. **21**(14): p. 2754-2763.
39. Sahoo, N.G., et al., *Functionalized carbon nanomaterials as nanocarriers for loading and delivery of a poorly water-soluble anticancer drug: a comparative study*. *Chemical communications*, 2011. **47**(18): p. 5235-5237.
  40. Kakran, M., et al., *Functionalized graphene oxide as nanocarrier for loading and delivery of ellagic acid*. *Current medicinal chemistry*, 2011. **18**(29): p. 4503-4512.
  41. Liu, Z., et al., *PEGylated nanographene oxide for delivery of water-insoluble cancer drugs*. *Journal of the American Chemical Society*, 2008. **130**(33): p. 10876-10877.
  42. Depan, D., J. Shah, and R. Misra, *Controlled release of drug from folate-decorated and graphene mediated drug delivery system: synthesis, loading efficiency, and drug release response*. *Materials Science and Engineering: C*, 2011. **31**(7): p. 1305-1312.
  43. Lu, Y.-J., et al., *Improving thermal stability and efficacy of BCNU in treating glioma cells using PAA-functionalized graphene oxide*. *International journal of nanomedicine*, 2012. **7**: p. 1737.
  44. Hasanzadeh, M., et al., *Determination of lisinopril using  $\beta$ -cyclodextrin/graphene oxide-SO<sub>3</sub>H modified glassy carbon electrode*. *Journal of Applied Electrochemistry*, 2014. **44**(7): p. 821-830.
  45. Soleymani, J., et al., *A new kinetic-mechanistic approach to elucidate electrooxidation of doxorubicin hydrochloride in unprocessed human fluids using magnetic graphene based nanocomposite modified glassy carbon electrode*. *Materials science and engineering: C*, 2016. **61**: p. 638-650.
  46. Yang, K., et al., *Graphene in Mice: Ultrahigh In Vivo Tumor Uptake and Efficient Photothermal Therapy*. *Nano Letters*, 2010. **10**(9): p. 3318-3323.
  47. Park, S., et al., *Biocompatible, robust free-standing paper composed of a TWEEN/graphene composite*. *Advanced Materials*, 2010. **22**(15): p. 1736-1740.
  48. Ku, S.H. and C.B. Park, *Myoblast differentiation on graphene oxide*. *Biomaterials*, 2013. **34**(8): p. 2017-2023.
  49. Lee, W.C., et al., *Cell-assembled graphene biocomposite for enhanced chondrogenic differentiation*. *Small*, 2015. **11**(8): p. 963-969.
  50. Lee, W.C., et al., *Origin of Enhanced Stem Cell Growth and Differentiation on Graphene and Graphene Oxide*. *ACS Nano*, 2011. **5**(9): p. 7334-7341.
  51. Li, N., et al., *Three-dimensional graphene foam as a biocompatible and conductive scaffold for neural stem cells*. *Scientific Reports*, 2013. **3**: p. 1604.
  52. Mukherjee, S., et al., *Graphene oxides show angiogenic properties*. *Advanced healthcare materials*, 2015. **4**(11): p. 1722-1732.
  53. Peer, D., et al., *Nanocarriers as an emerging platform for cancer therapy*. *Nature nanotechnology*, 2007. **2**(12): p. 751.
  54. Chen, J., X. Wang, and H. Han, *A new function of graphene oxide emerges: inactivating phytopathogenic bacterium *Xanthomonas oryzae* pv. *Oryzae**. *Journal of nanoparticle research*, 2013. **15**(5): p. 1658.
  55. Paek, S.M., J.M. Oh, and J.H. Choy, *A Lattice-Engineering Route to Heterostructured Functional Nanohybrids*. *Chemistry—An Asian Journal*, 2011. **6**(2): p. 324-338.
  56. Liu, L.-H., et al., *Advanced nanohybrid materials: surface modification and applications*. *Journal of Nanomaterials*, 2012. **2012**.
  57. Majno, G., *The healing hand: man and wound in the ancient world*. 1991:

- Harvard University Press.
58. Doshi, J. and D.H. Reneker, *Electrospinning process and applications of electrospun fibers*. Journal of electrostatics, 1995. **35**(2-3): p. 151-160.
  59. Formhals, A., *US patent 1975504*. 1934.
  60. Seaman, S., *Dressing selection in chronic wound management*. Journal of the American Podiatric Medical Association, 2002. **92**(1): p. 24-33.
  61. Augustine, R., N. Kalarikkal, and S. Thomas, *Role of wound dressings in the management of chronic and acute diabetic wounds*. Diabetes Mellit Hum Health Care Holist Approach Diagn Treat, 2014: p. 273-314.
  62. Biondi, M., et al., *Nanoparticle-integrated hydrogels as multifunctional composite materials for biomedical applications*. Gels, 2015. **1**(2): p. 162-178.
  63. Annabi, N., et al., *25th anniversary article: Rational design and applications of hydrogels in regenerative medicine*. Advanced materials, 2014. **26**(1): p. 85-124.
  64. Guarnieri, D., et al., *Effects of fibronectin and laminin on structural, mechanical and transport properties of 3D collagenous network*. Journal of Materials Science: Materials in Medicine, 2007. **18**(2): p. 245-253.
  65. Biondi, M., et al., *Controlled drug delivery in tissue engineering*. Advanced drug delivery reviews, 2008. **60**(2): p. 229-242.
  66. Vashist, A., et al., *Recent advances in hydrogel based drug delivery systems for the human body*. Journal of Materials Chemistry B, 2014. **2**(2): p. 147-166.
  67. Yue, K., et al., *Synthesis, properties, and biomedical applications of gelatin methacryloyl (GelMA) hydrogels*. Biomaterials, 2015. **73**: p. 254-271.
  68. Gkikas, M., R.K. Avery, and B.D. Olsen, *Thermoresponsive and Mechanical Properties of Poly*. 2016.
  69. Zhao, L., et al., *Antibacterial nano-structured titania coating incorporated with silver nanoparticles*. Biomaterials, 2011. **32**(24): p. 5706-5716.
  70. Kazemzadeh-Narbat, M., et al., *Antimicrobial peptides on calcium phosphate-coated titanium for the prevention of implant-associated infections*. Biomaterials, 2010. **31**(36): p. 9519-9526.
  71. Ma, M., et al., *Local delivery of antimicrobial peptides using self-organized TiO<sub>2</sub> nanotube arrays for peri-implant infections*. Journal of Biomedical Materials Research Part A, 2012. **100**(2): p. 278-285.
  72. Kazemzadeh-Narbat, M., et al., *Multilayered coating on titanium for controlled release of antimicrobial peptides for the prevention of implant-associated infections*. Biomaterials, 2013. **34**(24): p. 5969-5977.
  73. Kazemzadeh-Narbat, M., et al., *Antimicrobial peptide delivery from trabecular bone grafts*. Journal of Biomaterials and Tissue Engineering, 2014. **4**(11): p. 967-972.
  74. Shalumon, K., et al., *Sodium alginate/poly (vinyl alcohol)/nano ZnO composite nanofibers for antibacterial wound dressings*. International journal of biological macromolecules, 2011. **49**(3): p. 247-254.
  75. Vicentini, D.S., A. Smania Jr, and M.C. Laranjeira, *Chitosan/poly (vinyl alcohol) films containing ZnO nanoparticles and plasticizers*. Materials Science and Engineering: C, 2010. **30**(4): p. 503-508.
  76. Sudheesh Kumar, P., et al., *Flexible and microporous chitosan hydrogel/nano ZnO composite bandages for wound dressing: in vitro and in vivo evaluation*. ACS applied materials & interfaces, 2012. **4**(5): p. 2618-2629.
  77. Păunica-Panea, G., et al., *New collagen-dextran-zinc oxide composites for wound dressing*. Journal of Nanomaterials, 2016. **2016**: p. 34.

78. Mohandas, A., et al., *Exploration of alginate hydrogel/nano zinc oxide composite bandages for infected wounds*. International journal of nanomedicine, 2015. **10**(Suppl 1): p. 53.
79. Roh, D.-H., et al., *Wound healing effect of silk fibroin/alginate-blended sponge in full thickness skin defect of rat*. Journal of Materials Science: Materials in Medicine, 2006. **17**(6): p. 547-552.
80. Usman, A., et al., *Enhanced mechanical, thermal and antimicrobial properties of poly (vinyl alcohol)/graphene oxide/starch/silver nanocomposites films*. Carbohydrate polymers, 2016. **153**: p. 592-599.
81. Wen, X., et al., *In vitro and in vivo investigation of bacterial cellulose dressing containing uniform silver sulfadiazine nanoparticles for burn wound healing*. Progress in Natural Science: Materials International, 2015. **25**(3): p. 197-203.
82. Xiao, W., et al., *Synthesis and characterization of photocrosslinkable gelatin and silk fibroin interpenetrating polymer network hydrogels*. Acta biomaterialia, 2011. **7**(6): p. 2384-2393.
83. Zhou, L., et al., *Biomimetic mineralization of anionic gelatin hydrogels: effect of degree of methacrylation*. Rsc Advances, 2014. **4**(42): p. 21997-22008.
84. Sahoo, P., et al., *Magnetic behavior of reduced graphene oxide/metal nanocomposites*. Journal of Applied Physics, 2013. **113**(17): p. 17B525.
85. Wu, N., et al., *Synthesis of network reduced graphene oxide in polystyrene matrix by a two-step reduction method for superior conductivity of the composite*. Journal of Materials Chemistry, 2012. **22**(33): p. 17254-17261.
86. Si, S., et al., *A study of hybrid organic/inorganic hydrogel films based on in situ-generated TiO<sub>2</sub> nanoparticles and methacrylated gelatin*. Fibers and Polymers, 2013. **14**(6): p. 982-989.
87. Isner, J.M. and D.W. Losordo, *Therapeutic angiogenesis for heart failure*. Nature medicine, 1999. **5**(5): p. 491.

## **APPENDIX A: Poster Presentation 1**

### Abstract

- Non-healing or slow healing of chronic wounds is among the serious complications of diabetes.
- Decrease in the proliferation and migration of cells such as keratinocytes and fibroblasts is the major reason for the development of such chronic diabetic wounds.
- Multiple evidences have shown that graphene oxide (GO) and reduced graphene oxide possesses angiogenic property and promote wound healing by promoting proliferation and migration of fibroblasts and keratinocytes cells.
- Gelatin methacrylate (GelMA) based hydrogels display excellent hydrophilic properties due to the presence of hydrophilic groups in the polymer chains, which gives them highly porous, soft and flexible structure.
- In the current work, we have developed a reduced graphene oxide incorporated GelMA hydrogel dressing to improve wound healing by increasing proliferation and migration of cells as well as promoting formation of new blood vessels for increased supply of nutrients, oxygen and growth factors to wound area.

### Introduction

**Background**

- Approximately, 170 million people in the world has affected by diabetes [1].
- The foot ulcers in diabetic patients is a leading cause of amputation. [4].
- A delayed healing or non-healing of wound in a person with DFUs is due to the reduction of growth factor response and decreased cells, which lead to reduced peripheral blood flow and decreased angiogenesis.

**Solution**

- Recently, Graphene, Graphene oxide (GO) have attracted great interest in biomedical applications due to its potential to enhance angiogenesis in wound healing applications. [2].
- GelMA hydrogel contain excellent porous structure and hydrophilic properties to mimic the properties of natural extra cellular matrix (ECM).
- Hydrogels are biocompatible, non-antigenic, durable, permeable to water vapour, and maintain its physical structure even after excessive water absorption. [5-7].

**Aim of this study**

- In this study, GO incorporated GelMA hydrogel were synthesized using a simple UV crosslinking method.
- The hydrogels are then characterized (SEM, FTIR, TGF, DMA) to confirm the morphology of the material.
- The cytotoxicity of the hydrogel (Live/Dead, MTT assay) using hkeratinocytes cells confirmed the biocompatibility of the material.
- Finally, the wound healing scratch assay shows the ability of the material to promote faster healing of the wound.

### Materials and Methods

Pre-polymer solution of GelMA hydrogel was prepared following the method of Fatima et al [3]. 1%, 2% and 4% GO was dispersed in the GelMA solution and placed on a glass slide and then exposed to UV light (220 – 500 nm, 7.0 mW/cm<sup>2</sup>) for 10 seconds.

### Results and Discussions

- The images of SEM shows highly porous structure of hydrogels both in top and cross-sectional view as shown in fig. 1A and 1B. The Transmission Electron Microscopy (TEM) images of graphene oxide nanoparticles confirms the amorphous structure (fig. 1C and 1D).
- XRD spectra showed successful incorporation of rGO nanoparticles in GelMA hydrogels.
- The Live/Dead assay shows the cell viability up to 2% concentration of GO. No significant cytotoxic effect was observed up to 2% concentration of GO.
- that at 2% concentration of GO the wound was induced to closure comparatively to control, GelMA and 1% concentration of GO.
- GelMA hydrogel containing 2% rGO nanoparticles produced large number of blood vessels with highly branched capillary network in chick embryo model compared to Blank GelMA hydrogel treatment only.

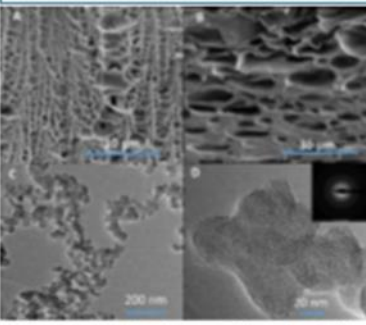


**Figure 1:** Fig. 1: (1): SEM micrograph (A) Top view of GelMA hydrogel (B) cross-sectional view of GelMA hydrogel. (C) GO nanoparticles (D) TEM image of amorphous GO nanoparticles.

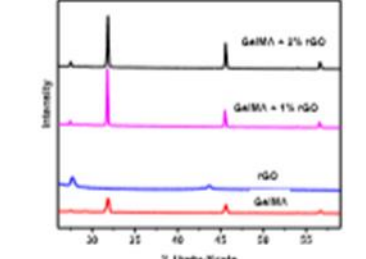


**Figure 2:** XRD of 2% rGO loaded GelMA hydrogel, 1% rGO loaded GelMA hydrogel, rGO and GelMA hydrogel respectively.

### Conclusions

- This rGO/GelMA hydrogel exhibited remarkable wound healing potential displaying improved keratinocytes proliferation and migration.
- GelMA hydrogel containing 2% rGO nanoparticles produced large number of blood vessels with highly branched capillary network in chick embryo model compared to Blank GelMA hydrogel treatment only.
- We strongly believe that our study on rGO/GelMA hydrogel will put forward the insight for the advancement of angiogenic treatment strategies for several diseases where angiogenesis plays a significant role.

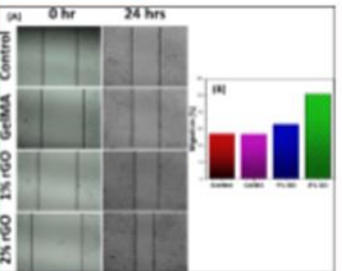


**Figure 3:** (A) Time dependant wound healing scratch assay of hkeratinocyte cells from 0 hour to 24 hours for control, GelMA hydrogel, 1% and 2% concentration of GO loaded GelMA hydrogel respectively. (B) Histogram of narrative result of percentage of migration of control, GelMA hydrogel, 1% and 2% concentration of GO loaded GelMA hydrogel respectively.

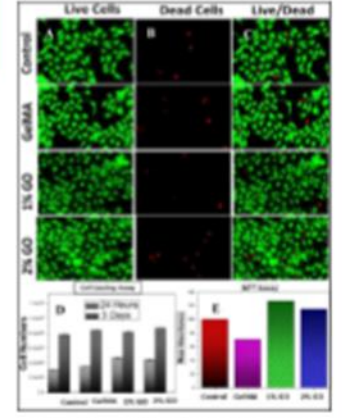


**Figure 4:** (A) Live Cells, (B) Dead Cells, (C) Live/Dead Cells, (D) Cell counting assay, (E) MTT assay of control, GelMA hydrogel, 1% GO loaded GelMA hydrogel, & 2% GO loaded GelMA hydrogel respectively.

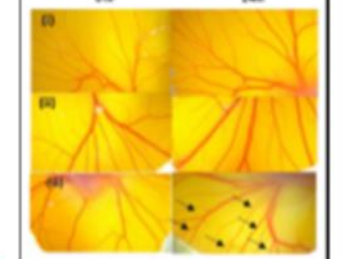


**Figure 5:** Blood vessel formation in chicken chorioallantoic membrane (CAM) assay after treatment of (i) pure GelMA (ii) GelMA with 1% rGO (iii) GelMA with 2% rGO.

### Acknowledgements

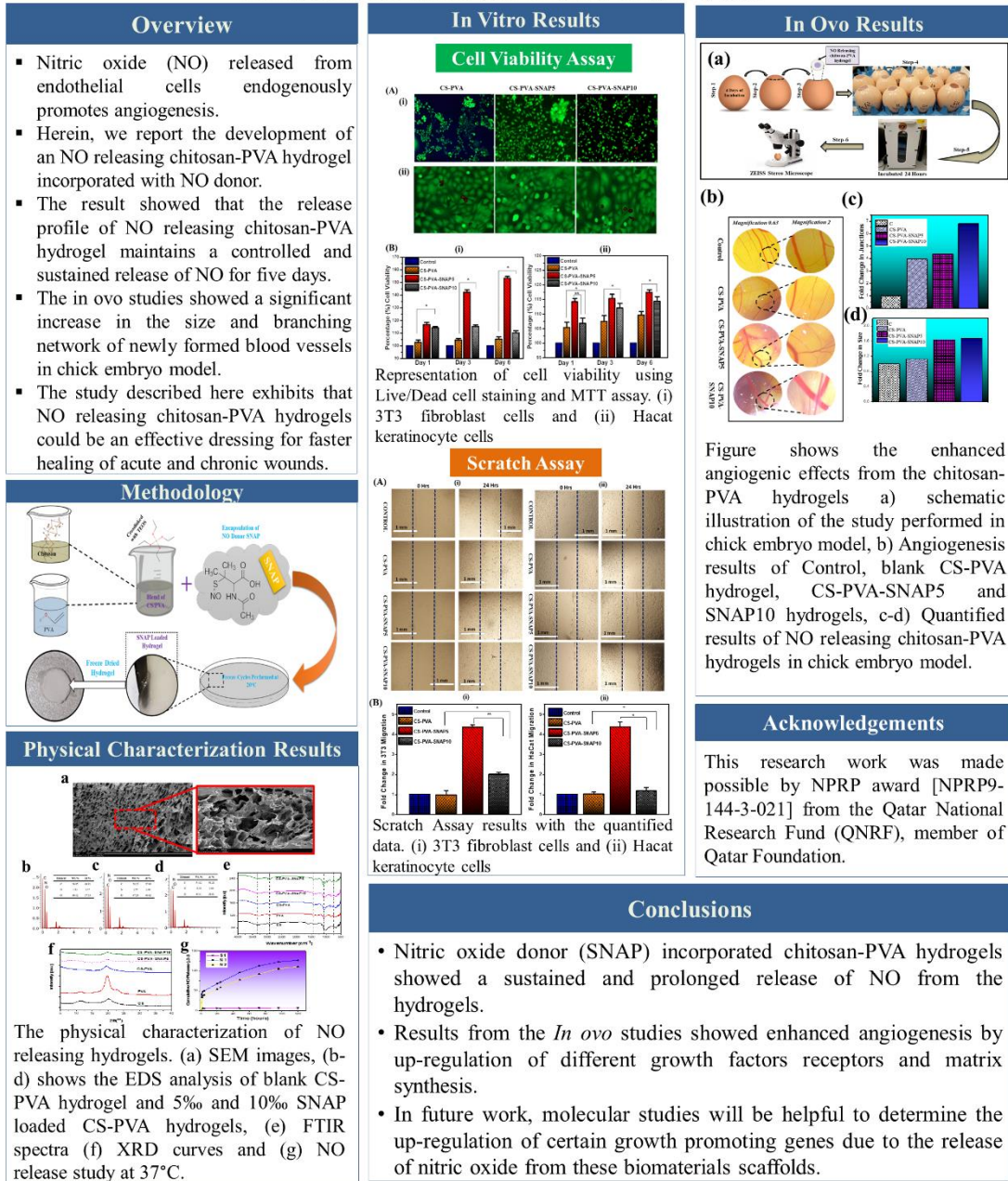
This research work was made possible by NPRP award [NPRP9-144-3-021] from the Qatar National Research Fund (QNRF), member of Qatar Foundation.

### References

- 1) WHO, S., et al., Global prevalence of diabetes: estimates for the year 2000 and projections for 2030. *Diabetes care*, 2004, 27(7): p. 1047-1053.
- 2) Mahajan, Advanced technology news/Ma, 2013, 4(1): p. 1722-1732.
- 3) El Hajj, Fatima, Advances in Biomedical Engineering (ICABME), 2013 International Conference, 2013, p. 144-142.
- 4) Rubin, J.E., E.J. Doyle, and D.G. Smith, Lower extremity foot ulcers and angiogenesis in diabetes. *Diabetes in America*, 1995, 8: p. 449-27.
- 5) Vishni, A., et al., Recent advances in hydrogel based drug delivery systems for the human body. *Journal of Materials Chemistry B*, 2014, 2(2): p. 147-166.
- 6) Bicerano, M., et al., Biofunctional collagen-based scaffolds embedding protein-releasing biodegradable microcapsules: using of porous release kinetics. *Journal of Materials Science: Materials in Medicine*, 2009, 20(10): p. 1128.
- 7) Mollica, F., et al., Mathematical modelling of the evolution of particle distribution within single PEGDA microcapsules: prediction of local concentration profiles and release kinetics. *Journal of Materials Science: Materials in Medicine*, 2010, 21(1): p. 157-159.

Alap Ali Zahid, Rashid Ahmed, Syed Raza ur Rehman, Robin Augustine, Anwarul Hasan

Department of Mechanical and Industrial Engineering, College of Engineering, Qatar University, Doha 2713, Qatar  
Biomedical Research Center, Qatar University, Doha, 2713, Qatar



**FOR MORE INFORMATION:** Dr Anwarul Hasan  
Assistant Professor, Department of Mechanical and Industrial, Engineering, Qatar University, Doha, Qatar, Email: ahasan@qu.edu.qa

## Graphene Oxide Loaded Hydrogel for Enhanced Wound Healing in Diabetic Patients

Syed Raza ur Rehman, Robin Augustine, Alap Ali Zahid, Rashid Ahmed, Anwarul Hasan.

**Abstract**— Several people with diabetes develop chronic wounds that are slow to heal or never heal. Decrease in the proliferation and migration of cells such as keratinocytes and fibroblasts is the major reason for the development of such chronic diabetic wounds. Therefore, designing a wound dressing patch using a biodegradable hydrogel which can provide a sustained release/delivery of active agents that can support cell proliferation and cell migration will be highly beneficial for promoting diabetic wound healing. Multiple evidences from both *in-vitro* and *in-vivo* studies have shown that graphene oxide (GO) and reduced graphene oxide promote wound healing by promoting proliferation and migration of fibroblasts and keratinocytes cells. In addition, rGO possesses angiogenic property. Gelatin methacrylate (GelMA) based hydrogels display excellent hydrophilic properties due to the presence of hydrophilic amido, amino, carboxyl and hydroxyl groups in the polymer chains, which gives them highly porous, soft and flexible structure. In this work, we report the development of hydrogel dressing incorporated with GO to improve wound healing by increasing proliferation and migration of cells.

### I. INTRODUCTION

Approximately, 170 million people in the world has effected by diabetes. Which includes 20.8 million people in the USA, and these numbers are projected to be double by 2030 [1]. The foot ulcers in diabetic patients is a leading cause of amputation. In the developed world, the hospital admissions and major morbidity are mostly associated with diabetes [2], which leads to pain, suffering, and a poor quality of life for the patients. 15% of the diabetic patients suffer from diabetic foot ulcers (DFUs), which leads to amputation and about 84% of all diabetic patients has lower-leg amputations [3]. The moment a diabetic patient suffers a wound in the skin of their foot, the became in danger of amputation. A delayed healing or non-healing of wound in a person with DFUs is due to the reduction of growth factor response and decreased cells, which lead to reduced peripheral blood flow and decreased angiogenesis. Recently, Graphene, Graphene oxide (GO) have attracted great interest in biomedical applications due to its potential to enhance angiogenesis in wound healing applications. Sudip mukharjee et al [4] observed angiogenic property of graphene oxide (GO) and reduced graphene oxide (rGO) through several *in-vitro* and *in-vivo* angiogenesis assays. They found GO and rGO exhibit pre-angiogenic property depending upon their concentrations. They also have suggested their study will be helpful in future development of Nano medicine. Whereas, GelMA hydrogel contain excellent

porous structure and hydrophilic properties to mimic the properties of natural extra cellular matrix (ECM). Hydrogels are cross-linkable synthetic or natural polymer chain. They have been widely applied in variation biomedical application such as regenerative medicine, tissue engineering and controlled drug delivery [5-9]. Their excellent hydrophilic property due to the presence of hydrophilic groups, such as amido, amino, carboxyl and hydroxyl in the polymer chains, makes them more feasible for wound healing application. This water content produces a highly porous, soft and flexible structure. Hydrogels are biocompatible, non-antigenic, durable, permeable to water vapour, and maintain its physical structure even after excessive water absorption. It securely covers the wound and prevents infection by bacteria. These all together make them quit similar to natural ECM. However, an ideal hydrogel should have stronger mechanical property, excellent antimicrobial activity.

In this study, GO incorporated GelMA hydrogel were synthesized using a simple UV crosslinking method. The hydrogels are then characterized (SEM, FTIR, TGF, DMA) to confirm the morphology of the material. The cytotoxicity of the hydrogel (Live/Dead, MTT assay) using hacat keratinocyte cells confirmed the biocompatibility of the material. And finally, the wound healing scratch assay shows the ability of the material to promote faster healing of the wound.

### II. METHOD

Pre-polymer solution of GelMA hydrogel was prepared following the method of Fatima et al [4]. 1%, 2% and 4% GO was dispersed in the GelMA solution and placed on a glass slide and then exposed to UV light (320–500 nm, 7.0 mWcm<sup>-2</sup>) for 10 seconds.

### III. RESULTS AND DISCUSSIONS

#### A. Scanning and Transmission Electron Microscopy (SEM & TEM):

The surface morphology of graphene oxide incorporated GelMA hydrogel were observed using Scanning Electron Microscopy. The images of SEM shows highly porous structure of hydrogels both in top and cross-sectional view as shown in fig. 1A and 1B. The Transmission Electron Microscopy (TEM) mages of graphene oxide nanoparticles confirms the amorphous structure (fig. 1C and 1D). However, the incorporation of graphene oxide in GelMA hydrogel doesn't make any difference in the morphology of hydrogel.

\* This article was made possible by the NPRP9-144-3-021 grant funded by the Qatar National Research Fund (a part of Qatar Foundation).

S. R. Rehman, R. Augustine, A. A. Zahid, R. Ahmed, and A. Hasan Author are with the Department of Mechanical and Industrial Engineering,

College of Engineering, Qatar University, Doha 2713, Qatar, and Biomedical Research Center, Qatar University, Doha, 2713, Qatar

\*Corresponding author: Anwarul Hasan, +97470569169.

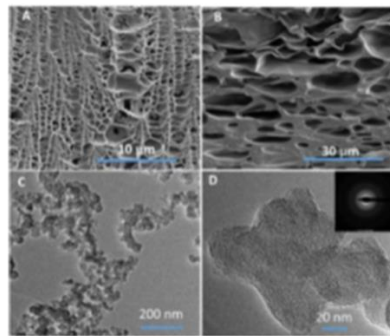


Fig. 1: Fig (1): SEM micrograph (A) Top view of GelMA hydrogel (B) cross-sectional view of GelMA hydrogel. (C) GO nanoparticles (D) TEM image of amorphous GO nanoparticles.

**B. Fourier-transform infrared spectroscopy (FTIR):**

The presence of graphene oxide is further confirmed by Fourier-transform infrared spectroscopy (FTIR) as shown in Fig. 2. The peaks of graphene oxide at wavelengths of 1589, 1229, 1163, and 846  $\text{cm}^{-1}$  can be seen in 2% GO loaded GelMA hydrogel plot. However, at less concentration of GO (0.5%) there is no significant changes in peaks, which confirms the incorporation of GO in GelMA hydrogel at 2% concentration.

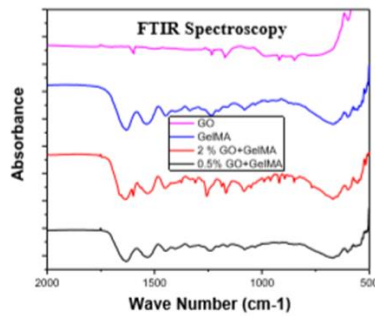


Fig. 2: Fourier-transform infrared spectroscopy (FTIR) of GO, GelMA hydrogel, 2% GO loaded GelMA hydrogel and 0.5% GO loaded GelMA hydrogel.

**C. Thermogravimetric Analysis (TGA):**

The thermal analysis of hydrogels by TGA demonstrates the stability of the hydrogel matrix to 239  $^{\circ}\text{C}$  as shown in fig. 3. There was initial weight loss due to loss of moisture in the gel from 30-80  $^{\circ}\text{C}$ . Since the GO loaded GelMA hydrogel is intended to be used for the release of drug from the hydrogel and the release process is normally carried out at physiological temperature 37  $^{\circ}\text{C}$ , the polymer is totally stable in the vicinity of room temperature which normally varies between 27 and 38  $^{\circ}\text{C}$ .

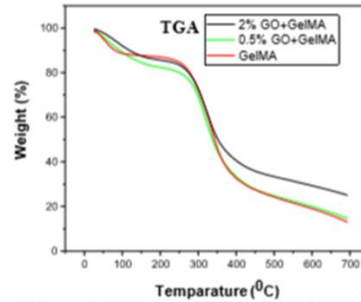


Fig. 3: Thermogravimetric Analysis (TGA) of 2% GO loaded GelMA hydrogel, 0.5% GO loaded GelMA hydrogel and only GelMA hydrogel respectively.

**D. Dynamic Mechanical Analysis (DMA):**

The dynamic mechanical analysis (DMA) are carried out to observe the difference in storage ( $G'$ ) and loss modulus ( $G''$ ) after the incorporation of GO in GelMA hydrogel. The amplitude and frequency sweep test (fig. 4A and 4B) reveals that the incorporation of GO has enhanced the viscoelastic properties of GelMA hydrogel. The ranges of storage and loss moduli for both amplitude and frequency sweep test is higher for 2% GO loaded GelMA hydrogel than only GelMA hydrogel.

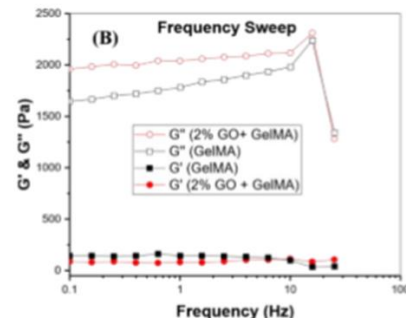
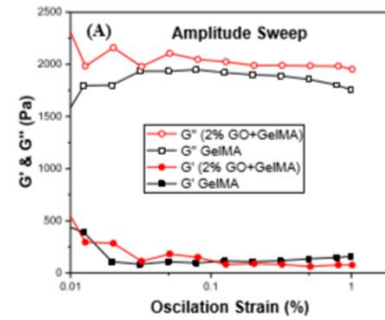


Fig. 4: The storage and loss modulus ranges in amplitude sweep test (4A) and frequency sweep test (4B) of GelMA hydrogel and GO loaded GelMA hydrogel.

#### E. *In-vitro* Cytotoxicity Assay:

The *in-vitro* cytotoxicity assay of the material is carried out using Live/Dead, cell counting and MTT assay (Fig. 5A, 5B, 5C, 5D, & 5E). The results clearly reveal the biocompatibility of the material. The Live/Dead assay shows the cell viability up to 2% concentration of GO. No significant cytotoxic effect was observed up to 2% concentration of GO. Also, the number of cells were counted after 1 day and 3 day of incubation using an automated cell counter. The histogram for the distribution of live/dead cells, based on cell size were then obtained using origin software (Fig. 5D). Overall results depict that the graphene oxide up to 2% concentration in GelMA hydrogel has almost no toxic effect on biocompatibility.

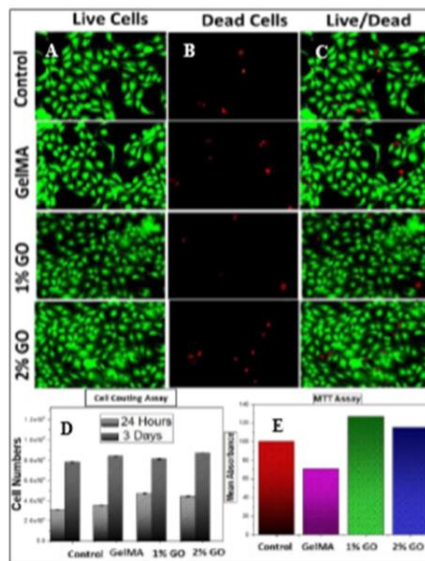


Fig. 5: (A) Live cells, (B) Dead Cells, (C) Live/Dead cells, (D) Cell counting assay, (E) MTT assay of control, GelMA hydrogel, 1% GO loaded GelMA hydrogel, & 2% GO loaded GelMA hydrogel respectively.

#### F. Wound Healing Scratch Assay:

Cell migration is one of the key steps in wound healing. A time dependent wound healing scratch assay was carried out from 0 to 24 hours in the presence of different concentration of GO. The result clearly depicts that at 2% concentration of GO the wound was induced to closure comparatively to control, GelMA and 1% concentration of GO. Comparatively to the controlled and GelMA hydrogel, the cells have migrated almost twice with 2% GO loaded GelMA hydrogel. The overall results suggested that the

GelMA hydrogel loaded with 2% of GO can enhance migration of hacat keratinocyte cells, indicating their pre-antigenic property.

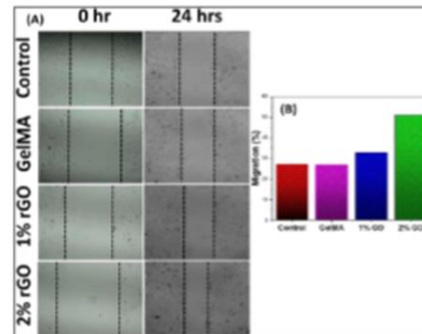


Fig. 6: (A) Time dependant wound healing scratch assay of hacat keratinocyte cells from 0 hours to 24 hours for control, GelMA hydrogel, 1% and 2% concentration of GO loaded GelMA hydrogel respectively. (B) Histogram of quantitative result of percentage of migration of control, GelMA hydrogel, 1% and 2% concentration of GO loaded GelMA hydrogel respectively.

#### IV. CONCLUSION

In this study, prepared GelMA hydrogel contains highly porous structures. The FTIR analysis confirmed the presence of GO GelMA hydrogel. Thermogravimetric Analysis (TGA) has shown the thermal stability of the hydrogel. Dynamic mechanical analysis (DMA) reveals that the incorporation of rGO has enhanced the viscoelastic properties of hydrogel. The *in-vitro* cytotoxicity studies confirmed the biocompatibility of the material. In addition, GO loaded GelMA hydrogel exhibited remarkable wound healing potential displaying improved keratinocytes proliferation and migration particularly at 2% concentration of GO. We strongly believe that our study on GO/GelMA hydrogel will put forward the insight for the advancement of wound healing treatment strategies in future.

#### REFERENCES

1. Wild, S., et al., *Global prevalence of diabetes: estimates for the year 2000 and projections for 2030*. *Diabetes care*, 2004. 27(5): p. 1047-1053.
2. Reiber, G.E., et al., *Causal pathways for incident lower-extremity ulcers in patients with diabetes from two settings*. *Diabetes care*, 1999. 22(1): p. 157-162.
3. Reiber, G.E., E.J. Boyko, and D.G. Smith, *Lower extremity foot ulcers and amputations in diabetes*. *Diabetes in America*, 1995. 2: p. 409-27.
4. Mukherjee, S., et al., *Graphene oxides show angiogenic properties*. *Advanced healthcare materials*, 2015. 4(11): p. 17221732.
5. Vashist, A., et al., *Recent advances in hydrogel based drug delivery systems for the human body*. *Journal of Materials Chemistry B*, 2014. 2(2): p. 147-166.
6. Biondi, M., et al., *Bioactivated collagen-based scaffolds embedding protein-releasing biodegradable microspheres: tuning of protein release kinetics*. *Journal of Materials Science: Materials in Medicine*, 2009. 20(10): p. 2117-2128.